UNIVERSIDADE TÉCNICA DO ATLÂNTICO
INSTITUTO DE ENGENHARIA E CIÊNCIAS DO MAR

WEST AFRICAN SCIENCE SERVICE CENTRE ON CLIMATE CHANGE AND ADAPTED LAND USE

Master Thesis

INVESTIGATING COASTAL SEA LEVEL VARIABILITY OF THE CAPE VERDE ARCHIPELAGO IN THE FACE OF CLIMATE CHANGE

SAMUEL MINTAH AYIM

Master Research Program on Climate Change and Marine Sciences

São Vicente
2021

UNIVERSIDADE TÉCNICA DO ATLÂNTICO
INSTITUTO DE ENGENHARIA E CIÊNCIAS DO MAR

WEST AFRICAN SCIENCE SERVICE CENTRE ON CLIMATE CHANGE AND ADAPTED LAND USE

Master Thesis

INVESTIGATING COASTAL SEA LEVEL VARIABILITY OF THE CAPE VERDE ARCHIPELAGO IN THE FACE OF CLIMATE CHANGE

SAMUEL MINTAH AYIM

Master Research Program on Climate Change and Marine Sciences

Supervisor | DR. JOHANNES KARSTENSEN

São Vicente
2021

UNIVERSIDADE TÉCNICA DO ATLÂNTICO
INSTITUTO DE ENGENHARIA E CIÊNCIAS DO MAR

WEST AFRICAN SCIENCE SERVICE CENTRE ON CLIMATE CHANGE AND ADAPTED LAND USE

Investigating coastal sea level variability of the Cape Verde archipelago in the face of climate change

Samuel Mintah Ayim

Master's thesis presented to obtain the master's degree in Climate Change and Marine Sciences, by the Institute of Engineering and Marine Sciences, Atlantic Technical University in the framework of the West African Science Service Centre on Climate Change and Adapted Land Use

Supervisor

Dr. Johannes Karstensen
Helmholtz Centre for Ocean Research, Kiel
(GEOMAR)

São Vicente
2021

UNIVERSIDADE TÉCNICA DO ATLÂNTICO
INSTITUTO DE ENGENHARIA E CIÊNCIAS DO MAR

WEST AFRICAN SCIENCE SERVICE CENTRE ON CLIMATE CHANGE AND ADAPTED LAND USE

Investigating coastal sea level variability of the Cape Verde archipelago in the face of climate change

Samuel Mintah Ayim

Panel defense

President

_____

Examiner 1

_____

Examiner 2

_____

São Vicente
Year

Financial support

The German Federal Ministry of Education and Research (BMBF) in the framework of the West African Science Service Centre on Climate Change and Adapted Land Use (WASCAL) through WASCAL Graduate Studies Programme in Climate Change and Marine Sciences at the Institute for Engineering and Marine Sciences, Atlantic Technical University, Cabo Verde.

Dedication

This work is dedicated to my family that has served as emotional shock absorber throughout my twenty-five years prior to this work. Especially to my dad, Chief Inspector in the Ghana Police Service, Samuel Ayim Mintah who prioritized my early educational years rather than gathering up riches for himself and for giving me the freedom to pursue a career according to my passion and not what the prevailing culture dictated.

Acknowledgements

I am exceedingly grateful to the almighty God for good health during this study period in the face of global adversity.

This work would not have been possible without my supervisor, Dr. Johannes Karstensen of the Helmholtz Centre for Ocean Research Kiel (GEOMAR), who despite his busy schedule found time for me always and gave guidance within the scope of the work and in career decisions. I am most grateful for the leadership.

I am thankful to the director of the WASCAL programme, Dr. Corrine Almeida (Instituto de Engenharia e Ciências do Mar (ISECMAR)) who was on-hand anytime I needed clarity and guidance. Special appreciation also to the scientific coordinator, Dr. Estanislau Baptista Lima who kept pushing me to ensure I finished this work before the stipulated deadline as well as the deputy Director Dr. Antonio Pinto and all the WASCAL staff.

Regards also to Dr. Gael Alory (LEGOS-OMP, Toulouse), Prof. Ursula Schauer (Alfred Wegener Institute, Bremerhaven), Prof. Nilton Manuel Évora do Rosário (Federal University of São Paulo (UNIFESP)) and Dr. Rainer Kiko (Laboratoire d'Océanographie de Villefranche-sur-mer), who taught courses that served as a primary foundation for this work. I am thankful to all the other lecturers as well and to all the numerous guys who have developed various Python computational solutions and have made it freely available online via Github.

Lastly, I am grateful to my colleagues of the WASCAL Cape Verde first batch for providing friendship during a time of studying in another country in the midst of a global pandemic.

Resumo

A costa está sujeita a um nível do mar variável desde uma escala de segundos a séculos. Este estudo quantifica os factores de variabilidade do nível do mar costeiro de Cabo Verde.Ao utilizar o único marégrafo público disponível em Palmeira, Sal (de Março de 2000 a Dezembro de 2019), estima-se a contribuição relativa das marés, picos, ondas de superfície e alterações do nível do mar impulsionadas pelas correntes oceânicas (topografia dinâmica). Uma análise espectral revelou que as marés (M2, S2, etc.) contribuem até 815mm da variabilidade do nível do mar observada de 1300 mm. O nível do mar em Palmeira com o sinal da maré removido revela uma variabilidade plurianual com uma magnitude de cerca de 212mm. Os picos e baixos identificados a curto prazo podem acrescentar mais 155mm, com a duração de algumas horas. Os produtos operacionais das ondas e do nível do mar revelaram que a maior variabilidade do nível do mar em Cabo Verde é devida às ondas (em média 1700mm e 4400mm em alguns casos) em escala temporal <12 segundos e foram principalmente impulsionados pelo vento. As tendências a longo prazo para o período de estudo foram de 2,238mm/ano, 3,024mm/ano e -0,156mm/ano para a reanálise CMEMS, satélite e marégrafo, respectivamente.As alturas dinâmicas SLA baseadas em satélite tinham um alcance de 182 e 208mm para o satélite e conjuntos de dados de reanálise com fortes ligações ao SST da região e à ondulação de tensão do vento. Uma extensão da rede de observação do marégrafo para a região de Cabo Verde ajudaria a verificar os produtos operacionais aqui utilizados e, assim, ajudaria a criar uma monitorização espacial do nível do mar na região de Cabo Verde. Serviços como as fábricas de dessalinização, portos locais, empresas costeiras, etc. beneficiariam de tal rede, para planeamento e operações.

Palavras-chave: Variabilidade do Nível do Mar, Marés, Ondas, Surtos, Topografia Dinâmica, Altimetria de Satélite, Alterações Climáticas, CMEMS.

Abstract

The coast which serves as an intermediary between land and the ocean is subject to variable sea level from a scale of seconds to centuries. This study quantifies the drivers for coastal sea level variability of Cape Verde. By making use of the only public available tide gauge at Palmeira, Sal (spanning March 2000 to December 2019), the relative contribution of tides, surges, surface waves and sea level changes driven by ocean currents (dynamic topography) are estimated. A spectra analysis revealed that the tides (M2, S2, etc.) contribute up to 815mm of the 1300 mm range in observed sea level variability. Further analyzing the sea level at Palmeira with the tidal signal removed (SLA_residual) reveals multiannual variability with a magnitude of about 212mm. Furthermore, identified event-like, short term surges and lows may add another 155mm, lasting a few hours. Operational wave and sea level products revealed that Cape Verde's highest sea level variability is due to waves (averagely 1700mm and 4400mm in some instances) in temporal scale <12 seconds and were primarily wind driven. The long term trends for the study period were 2.238mm/year, 3.024mm/year and -0.156mm/year for the CMEMS reanalysis, satellite and tide gauge, respectively. The satellite based dynamical heights sea level anomaly had a range of 182 and 208mm when using the satellite and reanalysis datasets with strong connections to the region's SST and wind stress curl. An extension of the tide gauge observational network for the Cape Verde region would help verify the operational products used here and thus help to create a spatial monitoring of the sea level in the Cape Verde region. Services such as the desalination-plants, local harbors, coastal businesses, etc. would benefit from such a network, for planning and operations.

Keywords: Sea Level Variability, Tides, Waves, Surges, Dynamic Topography, Satellite Altimetry, Climate Change, CMEMS.

Abbreviations and acronyms

ADCP	Acoustic Doppler Current Profiler
CMEMS	Copernicus Marine Service
FFT	Fast Fourier Transform
HR	High Resolution
mm	Millimeters
OTIS	OSU Tidal Inversion Software
SLA	Sea Level Anomaly
SSH	Sea Surface Height
SWH	Significant Wave Height
TOPEX	Ocean Topography Experiment
TPXO	Topex Poseidon crossover solution
WAM	Wave Model

General Index

Figure index

Table index

1. Introduction

1.1 Background and Context

The desire to live in coastal regions and areas has been one that goes back to centuries of years in time and it is one that is ever growing. However, coastal disasters such as storm surges and flooding threaten the lives and economy of coastal dwellers. Understanding the factors that determine coastal sea-level variability is of utmost important for coastal management and human well-being. According to IPCC (2014), the frequency, intensity and duration of extreme weather events is expected to increase. This increase in extreme weather events like stronger storms tends to enforce waves which in-turn impacts coastal communities. Kirshen et al. (2008), National Research Council (2009) and NOAA (2018) point out how a storm event can lead to coastal flooding primarily for low lying coastal communities through enormous wave pounding or sea-level elevations. Natural barriers like coral reefs and coastal defence structures like sea walls tend to protect some coast but when wave conditions are stronger than usual, these defences can be made null. Coastal defences and natural barriers can be: (a) breached or undermined, (b) overtopped by waves or (c) exceeded by water levels at its crest, which would lead to coastal flooding (Sallenger, 2000; Zou et al., 2013). Knowing how wave conditions and sea-level changes can create damaging consequences for coastal communities, it is prudent to have an idea of the wave situation and the sea-level variability within a coastal region so as to be able to understand past conditions which forms a basis to predict future scenarios.

In other to better understand factors that control sea-level conditions within a particular region, several sea-level observing approaches have been used by scientists and coastal states. These approaches vary but can be primarily grouped into two: (a) in-situ and (b) satellite observations. The in-situ observations include one of the oldest established sea-level observing methods which are tide-gauges and which go back more than 150 years at certain locations. One component that adds typically only short term but eventually extreme sea level signals are surface waves. These are lately integrated into numerical models to better understand the impact of waves (Janssen, 2008). To integrate limited in-situ data and satellite observations into a coherent picture and eventually predicting sea-level evolution, ocean models are used. One particular thread is expected from global warming through greenhouse gas emission, Church et al. (2013) predicts that global mean sea-level will increase of the order 0.3-1.0m by 2100 but locally the increases may be much higher. Storm flooding and inundation of lowland is one of four main impacts of sea-level rise (Nicholls, 2002). Thus,

with sea-level on a rise coupled with an increase in frequency, intensity and duration of extreme weather events, coastal nations may be on the verge of witnessing its greatest wave pounding in modern history.

1.2 Study Area

Cape Verde is located between the Equator and the Tropic of Cancer, between the latitudes 14°28'N and 17°12'N and the longitudes 22°40'W and 25°22'W, approximately 500km off the west coast of Senegal in West Africa. It has 10 islands with varying local climate conditions and landscape and elevations vary with mountains being more prominent on some than others. Sal island is the flattest island. With an annual temperature varying from 19 to 29°C, the Cape Verde has a tropical oceanic climate with low rainfall rates. The tidal range has been documented to be about a meter (Gomes et al., 2015). Cape Verde is loacted towards the southern end of the Canary Current and this has a southwestward flow around the area (Mittelstaedt, 1991).

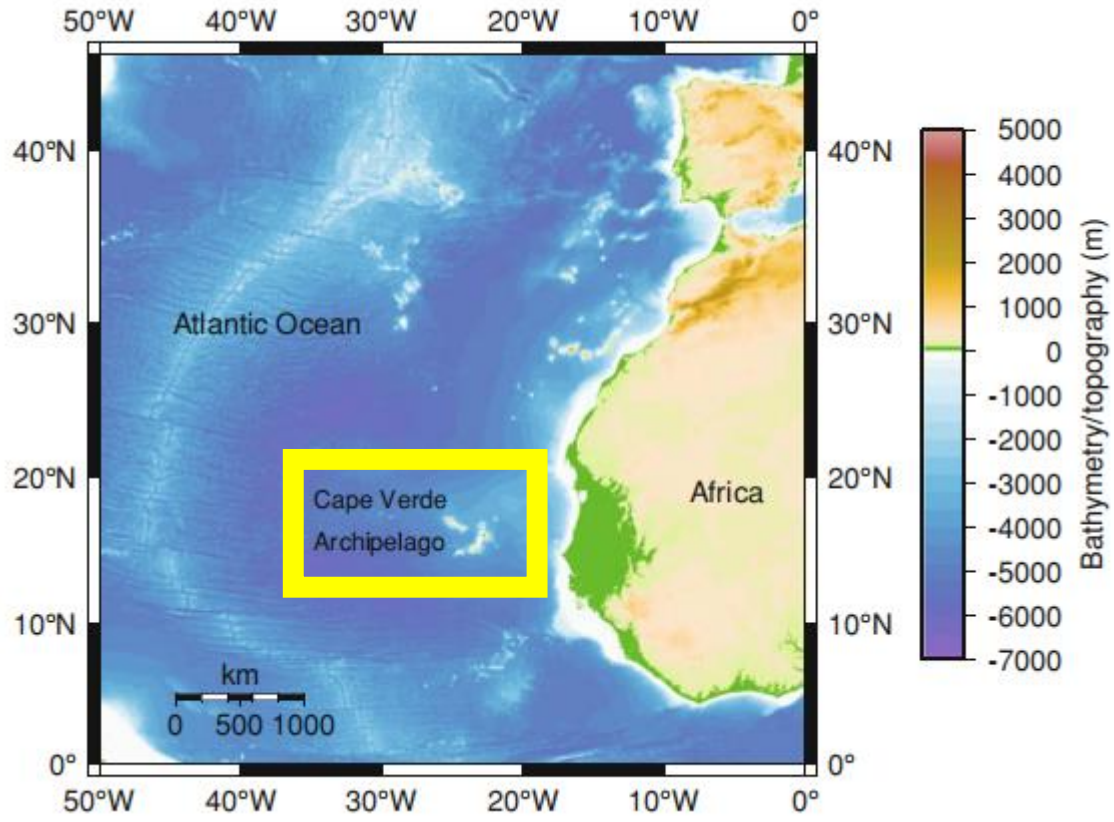

Figure 1: Map of the Cape Verde Islands location in reference to the African coast showing the bathymetry/topography of the region.. Sourced from: Romalho (2011).

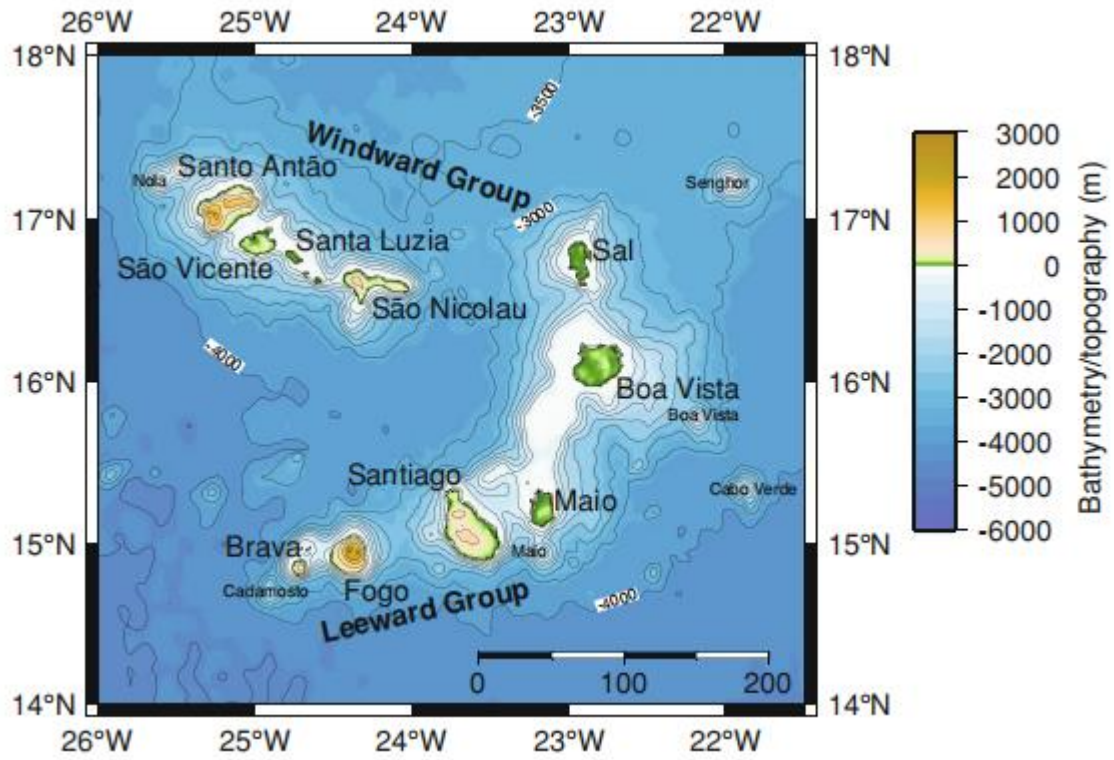

Figure 2: Map of Cape Verde showing the bathymetry and topography of the Islands and surrounding waters. The windward group is exposed to the prevailing local winds whiles the leeward group in the south are sheltered from the prevailing winds due to presense of the windward group. Sourced from: Romalho (2011).

1.3 Problem Statement

Understanding the factors that determine coastal sea-level variability is of utmost important for coastal management, safety and ultimately human well-being. This work seeks to identify and quantify the drivers for sea-level variability around the Cape Verde islands. Understanding the importance of what are supposed to be the main drivers for sea-level variability (namely, tides, surface waves, and variability in dynamic topography) will possibly help in planning for global (e.g. climate protection) and local (e.g. coastal protection) mitigation measures. For the Cape Verde region various natural hazards have been reported, such as erosion and gully formation for the island São Vicente (PANA 2004) or coastal flooding's induced by storms e.g. 2015 the impact of Hurricane "Fred" on the islands Sal and São Nicolau.

1.4 Research Questions

1. How large is the sea-level variability induced by tidal currents based on a local analysis for the Cape Verde Islands?
2. How large is the sea-level variability induced by surface waves and wind based on a regional analysis for the Cape Verde Islands?
3. How large is the regional and large scale sea-level variability induced by changes in dynamic topography for the Cape Verde Islands?
4. Which recommendations can be given for coastal management for the Cape Verde region related to sea-level variability based on the results?

1.5 Relevance and Importance of the Research

This research would give insights into the different factors that drive sea-level variability of the study area. The tidal variability, surface waves, and the dynamic topography are considered. Identifying and characterizing the main contributors of sea-level variability around the islands, is key for local and regional marine management issues such as coastal protection, operations of desalination plants, but also a base for potential wave energy power plants may be informed by the findings. Results of the findings are expected to be important for a wide range of individuals, organisations and government. Cape Verde's gross development product (GDP) in 2017 had tourism contributing 44.9% (WTTC, 2018), with the beaches being a prominent feature in the tourism sector. Coastal Hotels and businesses would also find it relevant as an understanding of the past conditions will help advice future measures. Policy makers, town planners and coastal users will all find it useful, knowing if a region is prone to harsh conditions. The country's electric power providers could also benefit.

2 Literature review

Sea-level variability can be accounted to a number of different drivers. In the following a literature review of the major drivers is provided.

2.1 Coastal Sea level

Coastal sea level refers to the water level recorded at any point in time along a shore (ocean-land interface). The sea level variability at the coast could be the same or different from that of the adjacent open ocean. One the reasons for this is the location of the coast and the timespan being considered (Woodworth et al., 2019). Coastal sea level have been studied over the years with the help of tide gauges while satellite observation gained significant grounds from 1993 (Dieng et al., 2019). The use of satellite gives a good representation of the open ocean but has drawbacks near the coast for varying reasons. One of which is radar echo perturbations caused by the continents (Cipollini et al., 2017). The advancement in instrumentation and post processing techniques implies that these challenges are been dealt with to improve the results of satellite observation of coastal sea level (Passaro et al., 2014; Birol et al., 2017).

Satellite and model data providers tend to want to validate their datasets with in-situ data; in this case tide gauge data. Validation for SLA data is extensive along the American and Western Europe coast as well as the Mediterranean Sea but poor along the African coast due to poor tide gauge network systems (Angnuureng et al., 2018). One of such African areas is the Eastern Tropical Atlantic Ocean, where the Cape Verde Islands is located.

A variety of oceanic phenomenon impacts coastal sea level such as surges, tides, waves, dynamic topography, etc.

2.1.1 Tides

The sun and moon's gravitational effect leads to a periodic and predictable changes in water level known as tides. Tidal ranges vary from one place to another with possibly the highest tidal range globally being 16m in the Bay of Fundy in Canada (Wolf, 2008). Locally tides are primarily monitored using tide gauges. In combination with other ocean phenomenon like surface waves and storm surges (Coles, 2001) the local and regional sea level characteristic and eventually forecast (in combination with numerical modelling) are derived. Satellite data provide long time barotropic tidal information for the global ocean (Ray, 1999).

Information on tides is important for many areas, e.g. tides are important for marine ecosystems related to mangroves (Gholami and Baharlouii, 2019) or Nodoushan (2018) pointed out the tidal impact on water quality. Ground elevation between group of islands act as barriers to tidal propagation and subsequently generates tidal velocities which are due to Coriolis inertia and advective inertia (Huthnance, 1973; Pingree and Maddock, 1980). These velocities can in-turn influence migration and abundance of larval and juvenile fish in estuaries (Embling et al., 2013; Patrick and Strydom, 2014; Abrogueña et al., 2020).

2.1.2 Surges

When water levels get high and overtops coastal defense structures or natural barriers leading to the inundation of a low-land as a result of tides, storm surges and wave action, coastal flooding is said to have occurred. Abe (1979) points out how earthquakes, meteorite, volcanic eruption or landslide can cause tsunamis which can also lead to coastal flooding and cites the classic example of the Pacific Rim. The risk of a coastal community having a flood event is projected to increase due to changing climate (Hall et al., 2007) and with coastal property being costly (Hinton et al., 2007), attention to coastal flooding seem to be ever critical. The impact of coastal flooding cannot be understated, countries have lost citizens (Gerritsen, 2005) whiles others have properties worth billions of euros sitting in zones at risk of coastal flooding (Wolf, 2008). This makes understanding the past situation of sea-level and waves even more prominent for a state such as the Cape Verde Islands which have some of its islands (example is Boa Vista) having a planar morphology with its highest peak being only 380m above sea-level (Romalho et al., 2010). Reports on coastal conditions such as flooding are sparse for the Cape Verde Islands but (Jenkins et al., 2018) did a great assessment of coastal flooding impacts as a result of the 2015 Hurricane Fred.

2.1.3 Surface Gravity Waves

Various types of energy input to the ocean propagate as surface gravity waves, meaning the restoring force is gravity. Best known are probably wind generated surface waves. Occasionally extreme surface waves may occur either from underwater landslides or triggered by earthquakes (tsunami) (Winter et al., 2017) or from intense storms such as hurricanes (Xiao et al., 2010). Measurements of surface waves directly with tide gauges and also with buoys either directly via the buoy motion (e.g. wave rider buoy, Tucker & Pitt, 2001) or via acoustic travel time from a subsurface instrument pointing upward (e.g. Nortek Signature 500 ADCP) (Hoitink et al., 2007). An important prerequisite is high sampling rate in order to be

able to resolve the wave frequency without an aliasing effect (Grédiac, 2014). These observations, also limited to a single region only, provide full statistics of the wave field (amplitude, frequencies) and which is of great value to characterize the regional surface waves. Remotely sensed wave observations include HR Radar observations (Chen et al., 2012) and Satellite altimetry. Both methods determine wave characteristics essentially from a backscatter signal. While HF Radar are stationary they can also be sued to derive areal information of wave characteristic. In contrast, satellite altimeters observe significant wave height (Hs) from the along track signal return which provides data at selected stripes in a region and for one moment only. The accuracy improved from first missions (e.g. TOPEX) being 10% or 0.5 m (whatever is larger) to better than 2% for SENTINEL-3 missions (Donlon et al., 2012). Satellite wave information is an important constrain for wave modelling that had its significant step when the 3rd generation (3G) Wave Model (WAM) was developed (Koeman, 1994). This did not lead to a stagnated growth as efforts to improve wave modelling are being made constantly. (The WISE group, 2007) worked on the development of shallow water physics which helps to better improve wave models. To better grasp the concept of numerical and statistical model as well as the design of coastal defences and oil platforms there needs to be enough accurate wave data (Casas-Prat et al., 2014; Durrant et al., 2013; Tolman, 2009; Comola et al., 2014; Kim and Suh, 2014). Others also estimate wave height by using results of radar images analysis which is however not straightforward. Radar images of the ocean helps to understand wave fields and surface current information (Chen et al., 2012; Nieto-Borge and Guedes-Soares, 2000) and these images are generated due to backscattering of electromagnetic waves as a result of sea surface roughness (Alpers and Hasselmann, 1982; Plant et al., 2008).

Due to the sparse nature of wave buoys and their relatively short-term deployment, most studies on the global ocean for wave trends on long-term scales tend to be mainly from voluntary observing ships, satellite altimetry, wave model hindcast and wave reanalysis datasets (Carter and Draper, 1988; Allan and Komar, 2000; Gulev and Grigorieva, 2004; Young et al., 2011). Doubts on the significant wave height measurements of Jason-2 have been raised but its relevance has been well documented by (Abdallah, 2019).

2.1.4 Dynamic Topography

The ocean surface tends to form hill and valley like structures in reference to the geoid. The sea surface height relative to the geoid is termed as the ocean's dynamic topography due to its fluidity. Satellite altimetry has been used to measure sea surface height from the 1990s

(Cazenave et al., 2014). Dynamic topography can lead to local variability in sea level (Bond, 1979). The accuracy of the current knowledge of the geoid information to help estimate the dynamic topography with precision is not enough (Caballero, 2020). The mean of dynamic topography is crucial in estimating sea level anomalies, however this estimation is said to be more accurate in the open ocean and decreases as one nears the coast (Caballero et al., 2020). One way to overcome the errors due to the geoid is by subtracting the mean sea surface above a reference ellipsoid from the from the sea surface height to obtain the sea level anomaly. An example of such works is being done by the Copernicus data team (Taburet et al., 2019).

2.1.5 Local Drivers

Coastal sea level variability can be driven by a lot of factors, some of which are local and introduces a variability in the local sea coastal sea level. Such forcing factors can be termed as local drivers as they vary depending on the location. Example of such drivers are the local bathymetry, shape of the coast, structures such as harbors, presence of estuaries and river run-offs (Woodworth et al., 2019). Most of these drivers have effect on smaller spatial scales and shorter temporal scales while others such as the Kelvin waves have a higher temporal and spatial scale (Enfield and Allen, 1980).

Bathymetry and the presence of a harbor or bay can induce an oscillation in the local waters known as seiches (Rabinovich, 2010). Seiches are sub-daily oscillations coastal sea level and have been found in almost all tide gauge records (Woodworth et al., 2019). The formula ($\sqrt{gh}$) where g is the acceleration due to gravity and h is the water depth, determines the frequency of a seiche.

River run-off also contribute to the local coastal sea level (Durand et al., 2019) with contribution of the order of centimeters for some European rivers (Laiz et al., 2014). River run-off will undoubtedly be significant in cases of larger rivers and vice versa. The Amazon River being a case of significant contributions from a large river (Korosov et al., 2015).

2.2 Interaction of drivers of Sea Level and Coastal Flooding

Oceanic motion phenomenon is a complex situation. These differently classed motions all interact with each other through diverse ways (Wolf et al., 1988). Peregrine and Jonsson (1983) classify these interactions as (a) effects of water levels and currents on waves and (b) effect of waves on tides and storm surges. This superposition of various drivers of sea level variability can lead to coastal flooding. Thus, a coastal defense system must take into account

the highest tide and highest probable waves of the target area in other to avoid wave overtopping during high wave conditions that are higher than usual. Coastal defense systems must take into account the interaction of these drivers of variability in sea level. An example is answering the question, will the structure be able to protect the coastal community when the highest wave occurs at the time of the highest tide? Understanding how nearshore zone wave propagation is modified by different tidal regimes is essential and this is detailed by (Wiegel, 1964; Wolf et al., 1988; Ozer et al., 2000). Wave propagation in the nearshore zone is dependent on the water depth, whiles wave breaking is also dependent on bottom friction. Thus, a wave entering a shallow area will shoal very close to land during low tide and slightly further from land during high tide.

In the nearshore, mean water level and flow is impacted by waves through radiation stress which causes longshore drift and wave setup (Longuet-Higgins and Stewart, 1962). Coastal defense managers and engineers in taking into account longshore drift would need to look at the question, what happens to the neighboring coast of the target coast. The understanding of these interactions has led to coupled models which tend to produce better output. An example of coupled models is the incorporation of current refraction in the WAM model (Hubert and Wolf, 1991). Burgers et al. (1994) and Cavaleri et al. (1994) detail contributions to coupling in the WAM project.

2.3 Impacts of Climate Change on Sea level Variability

Changes in temperature, sea level rise and ocean acidification are some of the threats of climate change to the marine environment ((Brierley and Kingsford, 2009; Doney et al., 2012; Hoegh-Guldberg and Bruno, 2010). Church et al., (2011) and IPCC (2013) indicate that melting of glaciers and ice-caps as well as ocean thermal expansion are the causes of sea-level rise. Sea-level is expected to increase by an order of 0.4m to 1.2m by 2100 (IPCC, 2013). Nicholls and Cazenave (2010) projects how the intertidal zone will undergo severe consequence as result of sea-level rise. This zone has great biodiversity and serve as buffer zones against storm events and erosion (Shepard et al., 2011; Spalding et al., 2014). The effect of climate change on marine organisms is however poorly understood (Richardson and Poloczanska, 2008; Rosenzweig et al., 2008). Estuaries would also be impacted primarily through salt intrusion (McLean et al., 2001).

Neumann et al., (2015) estimates that about 600million people live in areas that could be inundated. Thus, without protective measures, millions of people risk losing their homes

while coastal business would be hit hard. The transport industry such as the ports and road networks would also be impacted due to inundation as a result of sea-level rise (Becker et al., 2018; Dawson et al., 2016; Knot et al., 2017). Processes such as local changes in oceanic circulation, variability in ocean temperature and salinity, vertical land movement and static equilibrium cause regional sea-level changes to differ from global mean (Levermann et al., 2005; Kopp et al., 2014). This implies some countries will be more affected than others in the advent of sea-level rise. Sea-level rise is projected to impact the severity and frequency of coastal flooding (Talke et al., 2014). The impacts of climate change (sea-level rise) are certainly enormous with lives and properties at stake.

3 Data and Methods

3.1 Data Sources

A variety of datasets were used in this work. This includes in-situ tide gauge data from the University of Hawai'i sea level center and satellite and model data from the Copernicus Marine Service and the Copernicus Climate Change Service. Details of the datasets can be seen in Table 1.

Table 1: Summary of major datasets.

Data	Provider	Type	Temporal Resolution	Spatial Resolution	Time Span (d/m/year)	Location	Variables	Reference
Tide gauge	University of Hawai'i sea level centre.	In-situ	Hourly	Fixed location	12/03/2000 to 31/12/2019	16.755N to -22.98W		Caldwell et al. (2015)
Wind	Copernicus Climate Change Service	Reanalysis	Hourly	0.25degrees gridded	12/03/2000 to 31/12/2019	14 – 18N -22 to -26W	10m u & v-component	Hersbach et al. (2018)
Wave	Copernicus Marine Service	Reanalysis	3-Hour intervals	0.2degrees gridded	12/03/2000 to 31/12/2019	14 – 18N -22 to -26W	VHM0, VTM10 VMDR	Chune (2019)
Dynamic Topography	Copernicus Marine Service	Satellite observation	Daily	0.25degrees gridded	12/03/2000 to 31/12/2019	14 – 18N -22 to -26W	SLA	Mertz (2012)
Sea surface height	Copernicus Marine Service	Reanalysis	Daily	0.083degrees gridded	31/12/2019	14 – 18N -22 to -26W	Zos	Bourdalle (2012)

For the Copernicus datasets, the used variables are sea surface wave significant height [VHM0], sea surface wave mean period from variance spectral density inverse frequency moment [VTM10], sea surface wave from direction [VMDR], sea level anomalies [SLA], sea surface height [Zos].

The tide gauge data provided by the University of Hawai'i sea level center is located on the coast of Palmeira on the Sal Island. Palmeira is on the west coast of the Sal Island and the tide gauge is located in a bay which serves as the local harbour at 16°45'N, 22°59'W (Figure 3). There is a DORIS (Doppler Orbitography and Radiopositioning Integrated by Satellite) station about 5km away used in calibrating the Jason satellites. The tide gauge data is an amalgamation of three instruments; Aquatrak acoustic gauge, Sutron 9000 DCP, radar (Vega Vegapuls 62) and a pressure transducer. The acoustic device samples every 6 minutes

whiles the radar at 3 minutes and the pressure transducer at 2 minutes. The Aquatrak acoustic gauge was the primary sensor from March 2000 to 2007 and the radar is the current primary sensor since October 2007. The sampling technique is in a way which allows mechanical dampening of water level oscillations with periods of about 6 seconds (Park et al., 2014) which could eliminate the signal of some waves. The data providers use a three-point hanning filter centred on the hour to achieve the hourly observations used in this study. The units of the sea level observations is millimetres and it is referenced to a local station tide staff zero using land-based benchmarks. Thus, making its reference zero not relative to the local tidal parameters (Caldwell et al., 2015) or an official datum. It also makes the observations not start at a zero. The data contains some gaps of which no particular reason was given (Caldwell et al., 2015). The data is coded by the following identification numbers for various sources; (JASL: 235A, GLOSS: 329, NODC: 71026201). The island is affected by a -1.06mm/year vertical land motion (Mendes et al., 2017).

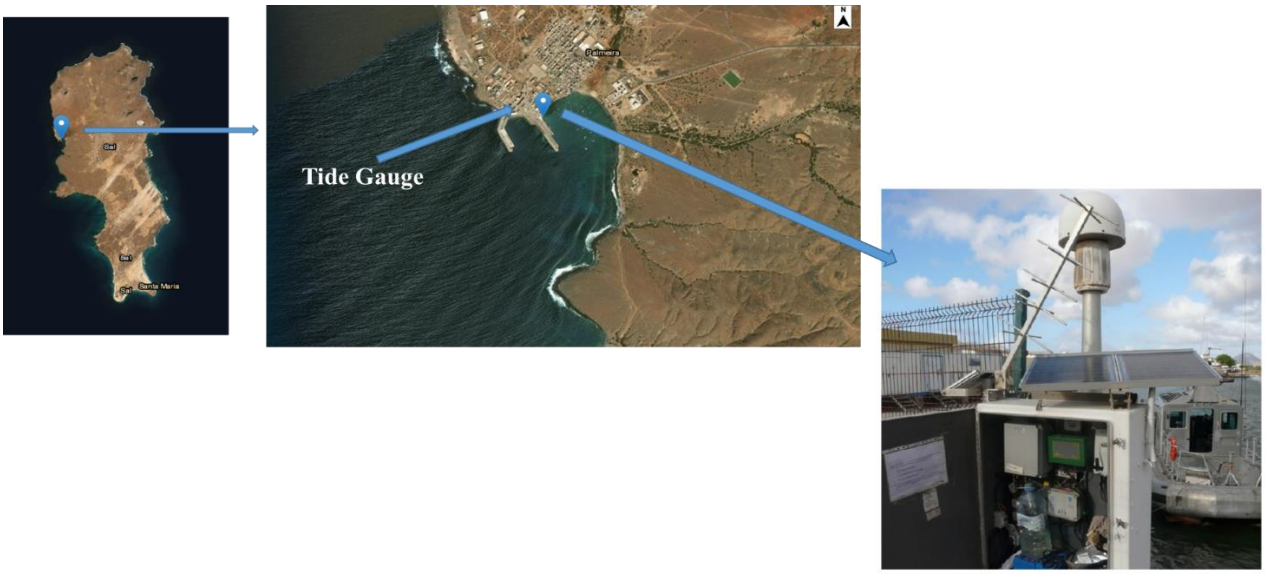

Figure 3: Site map of location of tide gauge (right) (blue locator on map) in the local habour of the city of Palmeira (centre) and its position in reference to the island (left). Sourceed from https://earthexplorer.usgs.gov/.

3.2 Major Python Packages Used

The python environment, provides various packages designed by thousands of individuals to help analyze various forms of data. A number of functions from these packages were used to analyze the various datasets. Below is a list of the packages that were used most times.

Table 2: Names of the major Python packages used in data analysis.

Datetime	Matplotlib	Numpy
Oceans	Os	Pandas
Pathlib	pyTMD	Pyproj
Scipy	Seaborn	Statsmodels
UTide	Windrose	Xarray

3.3 Tides

3.3.1 Unified Tidal Analysis and Prediction (UTide) Python Package

To estimate the local contribution of tidal frequencies on a time series I applied the UTide Python Package (Codiga, 2011). UTide performs a harmonic analysis of oceanic tides through a least-squares fit that considers the relative phase and amplitude of known tidal frequencies to an observational record, the Palmeria time series in this application.

First, the time series was prepared. A reference zero sea-level at the position of the gauge was computed by estimating the mean of the sea-level elevations of the study period. This mean value was subtracted from each sea-level elevation value to create a reference zero sea-level and obtain values of sea-level at each point in time as above or below the reference sea level. The "UTide" python package was then used to extract the tides from this preprocessed dataset by using the coefficients of the observations to reconstruct the tides (eqn 1). The utide.solve takes the raw time, sea level and the latitude of the gauge to generate various string, scalar and vector fields (coef) which contains information such as the constituents name, amplitude, Greenwich phase lag, contituents frequencies among many others. The utide.reconstruct function then take the time stamps and gleans information from the coef variable to reproduce the tides of the location over the inputted time.

$$\boldsymbol{coef = utide.solve(time, sea\ level_{observations}, lattiude\ of\ Tide\ Gauge)} \quad \textit{(1)}$$
$$\boldsymbol{tide = utide.reconstruct(time, coef)}$$

The residue was then computed by subtracting the tidal elevations obtained from the "UTide" package from the preprocessed sea-level observations. The residue is the sea-level devoid of tidal fluctuations.

$$\boldsymbol{Residue = Sealevel_{observations} - Tidal\ elevations} \quad \textit{(2)}$$

3.3.2 TPXO Model

The TPXO model (Egbert and Erofeeva, 2002) was used to attain the local tidal constituents and their amplitudes and to compare this output to that extracted from the tide

gauge data by the UTide package. The TPXO model of global ocean tides is generated by using the Laplace tidal equations and altimetry data. The Laplace equations is a set of partial differential equations which takes into account the lateral forcing by gravity and the Coriolis Effect. The model was run in python using the pyTMD python package's function "extract_tidal_constants". This function takes the location's longitude and latitude position as well as the path to the grid file (gf) and the model file (mf) and the coordinate system of the location as seen below where "TYPE" is set to 'z' to attain the amplitudes of the tidal constituents. Amplitude, phase, depth and constituents are amp, ph, D and c respectively. Grid is set to 'OTIS' which is the file type used while method set to spline is said to be the best as compared to linear interpolation method. The model file is generated by using a tidal synthesis program to compute for a given time and location, the tidal corrections (Egbert and Erofeeva, 2002).

$$\boldsymbol{amp, ph, D, c = pyTMD.read_{tide_{model}}.extract_{tidal_{constants}}(lon, lat, gf, mf, EPSG, TYPE = 'z',\ METHOD = 'spline', Grid = 'OTIS'} \quad \textit{(3)}$$

The TPXO model was also used to attain the tidal constituents and their amplitude for the Cape Verde region. To do so, 410 grid points were created for the Cape Verde region, the model was used to estimate the tidal constituents and amplitudes at those points. For each point (location), the sum of the amplitudes of the all the tidal constituents was estimated as a representative of the tidal range at the location. The mean was then estimated for the entire Cape Verde area and used as the representative of the tidal range of the region.

3.3.3 Spectral Analysis

A spectral analysis was carried out on the raw data and residue to cross-validate the analysis of the UTide package. The Fast Fourier Transform (FFT) of the "numpy" python package was used for the spectral analysis. The Fourier analysis transforms a signal from the more prominent time domain the frequency domain or vice versa. The goal was to visualize the frequency with the highest energies in the computed sea-level anomaly and the residue. Subsequently the energies of these two were compared to verify if the UTide package worked effectively in extracting the tidal signal. The power spectra is based on the algorithm (eqn 4) where N is the number of elements.

$$X_k = \sum_{n=0}^{N-1} x_n e e^{-2\pi i k n / N}) \quad (4)$$

The computation of the energies of the FFT in python followed this sequence;

$$hanning_{window} = numpy.hanning(length\ of\ data) \quad (5)$$

$$Power\ Spectrum_{Dataset} = numpy.fft.fft(hanning_{window} * Sealevel_{Anomaly}) \quad (6)$$

This computation leads to a two-sided spectrum, however, the focus is on positive frequencies. Thus, the two sided power spectrum was converted to a single sided power spectrum. The frequencies for the single sided power spectrum was also computed as seen below where Fs is the sampling rate in seconds and N is half the length of the data plus 1.

$$Frequency_{points} = numpy.linspace\ (0, \frac{Fs}{2}, N) \quad (7)$$

3.4 Surges and Extreme Lows

For the identification of surges and extreme low events, a two weeks high pass filter results of the residue was used. This was chosen to filter out everything above two weeks and identify the high and low events that occur in time scales of less than two weeks. The filtering was done with the lanczos filter from the "oceans" python package. The lanczos filter takes the input of the threshold frequency and window size to generate the weights as seen below.

$$Weights = ocean.filters.lanc(window_{size} * frequency_{threshold}) \quad (8)$$

After obtaining the weights, the residue and weights are used as the input argument for the numpy convolution with the mode set to same as seen below. This returns the low pass filter results (eqn 9). To obtain the high pass results, the low pass results is subtracted from the residue (eqn 10).

$$Low.Pass_{results} = numpy.convolve(Weights, Residue, mode = 'same') \quad (9)$$

$$High.Pass_{results} = Residue - Low.Pass\_results \quad (10)$$

This leads to a smoothing of all frequency signals at 14 days and above while preserving frequencies less than 14 days. After obtaining the high pass results of the residue, the time series of it was plotted and an amplitude of threshold of 4.3 times the standard deviation was set. Every point in the study period that had an amplitude greater than 4.3 times the standard deviation was classified as a surge (high event). Whiles those going lower than the negative of 4.3 times the standard deviation were classified as extreme low events.

In other to understand the events and possible causes, it is necessary to compare the high pass filtered residue sea level data used for the events identification in the previous section to datasets from possible drivers. One of a likely possible driver is the wind speed and direction. Hourly reanalysis wind data from Copernicus climate service was used to check the Pearson correlation between the wind speed and the high pass filtered data as well as the correlation between the wind direction and the high pass filtered data. The wind data primarily comes with only the u and v components. The wind speed and direction was computed using equations 11 and 12. The wind speed is the square root of the sum of the squares of the east-west (u) and north-south (v) component of the wind.

$$\boldsymbol{Wind_{speed} = np.sqrt(np.square(u_{component}) + (np.square(v_{component})))} \quad \textbf{(11)}$$

$$\boldsymbol{Wind_{Direction} = np.mod(180 + np.rad2deg(np.arctan2(v_{component}, u_{component})), 360)} \quad \textbf{(12)}$$

The Pearson correlation was then computed to show how the wind speed and direction are correlated to the high pass filtered data used for the events identification. The scipy python package was used to compute this as follows;

$$\boldsymbol{Correlation_{,\_} = scipy.stats.pearsonr(Wind_{speed}, High.Pass_{results})} \quad \textbf{(13)}$$

$$\boldsymbol{Correlation_{,\_} = scipy.stats.pearsonr(Wind_{Direction}, High.Pass_{results})} \quad \textbf{(14)}$$

Another possible driver for the surges or extreme low events could be waves. In other to understand this, the high pass filtered residue sea level data is compared with a 3-hourly Significant Wave Height (SWH) data from the Copernicus marine service. The Pearson correlation between the SWH data of tide gauge area and the high pass filtered data as well as the correlation between the filtered form of the SWH data and the high pass filtered data. However, since the wave data comes at 3-hourly timestamps as compared to the 1-hourly timestamps of the tide gauge data, the wave data was resampled into 1-hourly timestamps by interpolating the data between timestamps as seen below; where "H" is the resampling to hourly term.

$$\boldsymbol{Resample_{results} = Wave.Data_{dataframe}.resample("H").interpolate()} \quad \textbf{(15)}$$

After the interpolation, the correlation was computed.

$$\boldsymbol{Correlation_{,\_} = scipy.stats.pearsonr(SWH, High.Pass_{results})} \quad \textbf{(16)}$$

3.5 Waves

The CMEMS wave dataset was used to analyze the wave conditions of Cape Verde and its' contribution to the local sea level. Firstly, the significant wave height for the whole Cape Verde during the study period was juxtaposed against that of only Palmeira. This was done by finding the average SWH of the area at each point in time using loops in Python. The correlation for the two locations was then computed to ascertain how the local scale of Palmeira do compare to the whole Cape Verde region.

To further understand the behavioral relation of the two regions, the datasets were decomposed to extract the monthly seasonality having resampled the 3-hourly spaced dataset to monthly. This was computed using the seasonal decompose function from the statsmodel as seen below for Palmeria and Cape Verde.

$$\boldsymbol{Result = seasonal\_decompose(CV\_Data, model = 'addittive', extrapolate\_trend = 'freq', period = 12)} \quad \textit{(17)}$$

Having accessed the temporal variability of the Cape Verde SWH, the spatial variability for the study period was also investigated by computing the mean of each location over the entire study period and set into a filled contour plot using the cartopy python package. A wave rose was also generated with the windrose python package to understand the direction of the waves. Waves are not all about its height or direction but also its periodicity. What are the likely magnitudes of these three parameter? Does these magnitudes change if the waves are higher? To understand these, the seaborn python package was used to visualize the probability density function (PDF) of these three parameters for the whole dataset and for moments when the SWH was higher than or equal to 2,500mm (2.5meters).

3.6 Satellite based dynamical heights Sea-level Anomalies

The low-pass (periods > 2 weeks) filtered tide gauge data at Palmeira was then compared to satellite and model reanalysis dataset to observe how it compares with the sea-level (waters) of the entire Cape Verde. The CMEMS satellite observation of sea level anomaly and the CMEMS model reanalysis of sea surface height was used to compare. This was done by finding the mean sea-level of the area at each point in time using loops in Python while converting all units to millimeters. Correlations were computed between all the datasets.

Three types of events were identified in the Cape Verde model and tide gauge time series and analyzed by visualizing the model data maps of those moments in time. These events were moments in which sea-level was;

i. High in both the model and tide gauge time series.
ii. High in the model but low in the tide gauge time series.
iii. Low in the model but high in the tide gauge time series.

The trends in the sea level for all the time series were then generated using the signal function from the scipy package which performs a linear least squares fit to obtain the trend in the input dataset.

$$\boldsymbol{Trend = Sealevel_{Dataset} - signal.detrend(Sealevel_{Dataset})} \quad \textit{(18)}$$

The datasets were decomposed to extract the monthly seasonality having resampled the daily spaced two weeks filtered dataset to monthly. This was computed using the seasonal decompose (sd) function from the statsmodel with period indicating the number of one cycle;

$$\boldsymbol{Result = sd(Sealevel_{Dataset}, model = 'additive', extrapolate\_trend = 'freq', period = 12)} \quad \textit{(19)}$$

To check for possible divers of the sea level anomalies of Cape Verde, the seasonal cycle of the SLA was compared with sea surface temperature and wind stress curl of the region. The sea surface temperature product (Donlon et al., 2011) was decomposed into a monthly seasonal cycle. The wind stress curl was also obtained by using the Copernicus climate service's wind (u and v-component) product. Equations 20 to 22 were used to estimate the wind stress curl, where U and V are wind u & v-components, W is the wind speed, ρ_{air} is the air density, C_d is the drag coefficient (0.0017) and τ_x and τ_y are the zonal and meridional wind stress component.

$$\boldsymbol{\tau_x = \rho_{air} C_d W * U} \quad \textit{(20)}$$

$$\boldsymbol{\tau_y = \rho_{air} C_d W * V} \quad \textit{(21)}$$

$$\boldsymbol{Curl = \tau_y / d_x - \tau_x / d_y} \quad \textit{(22)}$$

4. Results

4.1. Sea level observations at Palmeira

The raw data file contained hourly sea level readings in millimeters for the tide gauge in Palmeira, Sal (Figure 4). This data had a range of 1,300mm over the study period (March 12, 2000 to December 31, 2019). The observations does not start from a zero because it is referenced to a local station tide staff zero using land-based benchmarks. Thus, making its reference zero not relative to the local tidal parameters (Caldwell et al., 2015). The observations are about 29.421 ± 0.008m (29,421 ± 0.000008mm) above the ellipsoid (PSMSL, 2021). Thus to obtain the sea level at Palmeira using the tide gauge in reference to the ellipsoid, one has to add 29,421mm to the observation of the said time.

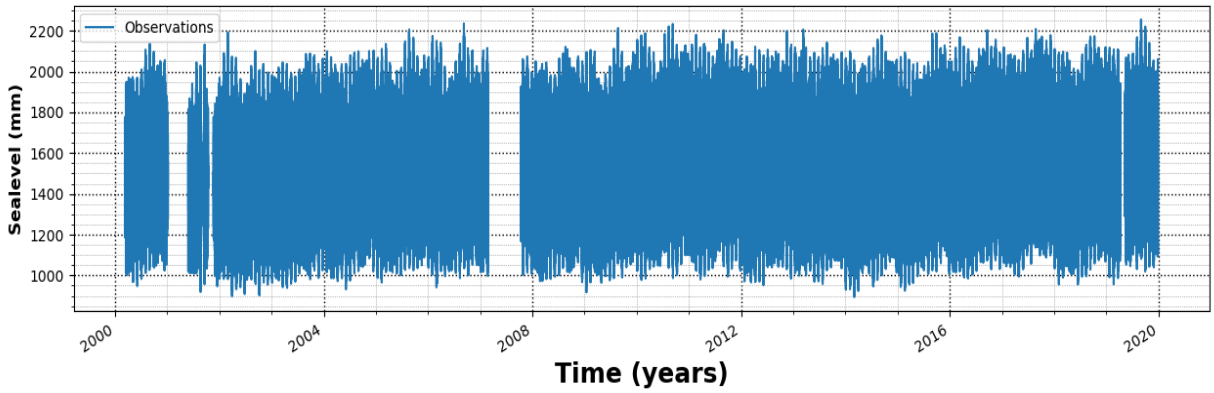

Figure 4:Times series of sea level observations from the tide gauge at Palmeira. Gaps are periods were no tidal records are available and was termed as missing values by University of Hawaii Sea level Centre.

The mean sea level is 1510mm with range of from 894 to 2254mm. Without the 10% of the highest and lowest data, the mean is 1510mm and range is from 896 to 2222mm. In the following we will decompose this signal into contributing forcing terms as outlined above.

In order to identify energy accumulation in certain frequency band of the sea level record (Figure 4) a spectral analysis is applied. The spectral analysis is based on a Fast Fourier Transformation (eqn 4, 5, 6, 7) and the spectral analysis showed (Figure 5) that energy peaks are at periods that match frequencies of tidal motions (Table 3).

What will be done in the following is to decompose the raw dataset of sea level variability into it potential drivers. First, we analyze the contribution from the most energetic contributor, which are the tides (Figure 6). After isolating the tidal signal a residual time series is obtained that is further analyzed for cases of surges and extreme low sea level events.

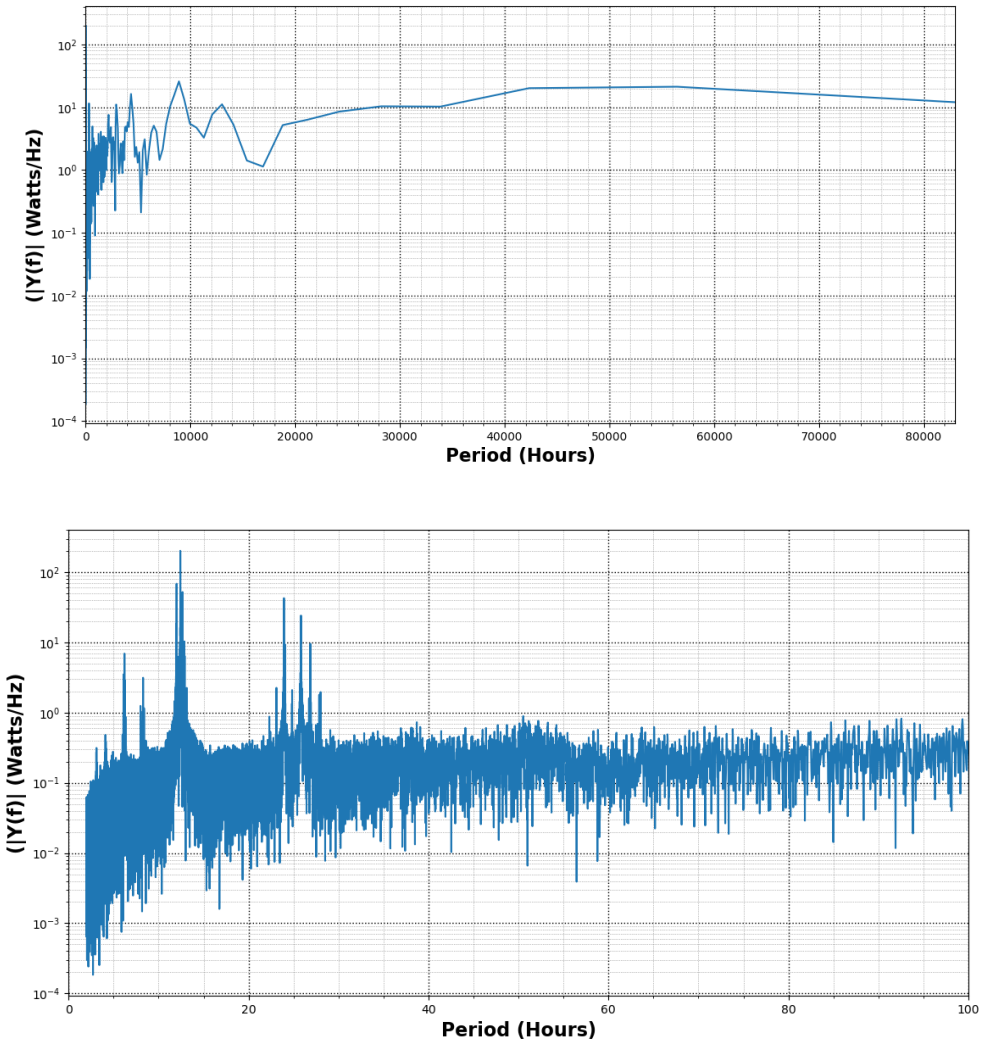

Figure 5: Spectral Analysis of the raw sea level data from the Palmeira tide gauge showing the energy of the various frequencies for half the sampling period (top) and for the first 100 hours (bottom).

4.2 Tides Induced Sea-level Variability

In order to isolate the tidal signal that dominates the spectral analysis (Figure 5), a decomposition into constituents was done by applying the "Unified Tidal Analysis and Prediction" (UTide) software package (Codiga, 2011). The UTide analysis showed the sea-level at Palmeira, Sal has a large contribution (about 815mm) from tides (Figure 6), also evident in the dominance of consistent oscillation of the sea level.

The UTide package does not only derive the tidal fit but also the individual tidal constituents and the amplitude of each. The analysis of the tide gauge data in Palmeira resulted in 68 individual constituents with the principal semidiurnal lunar tide (M2) being the dominating tide, contributing over twice (Table 3) the second highest contributing tide (principal solar semidiurnal tide, S2).

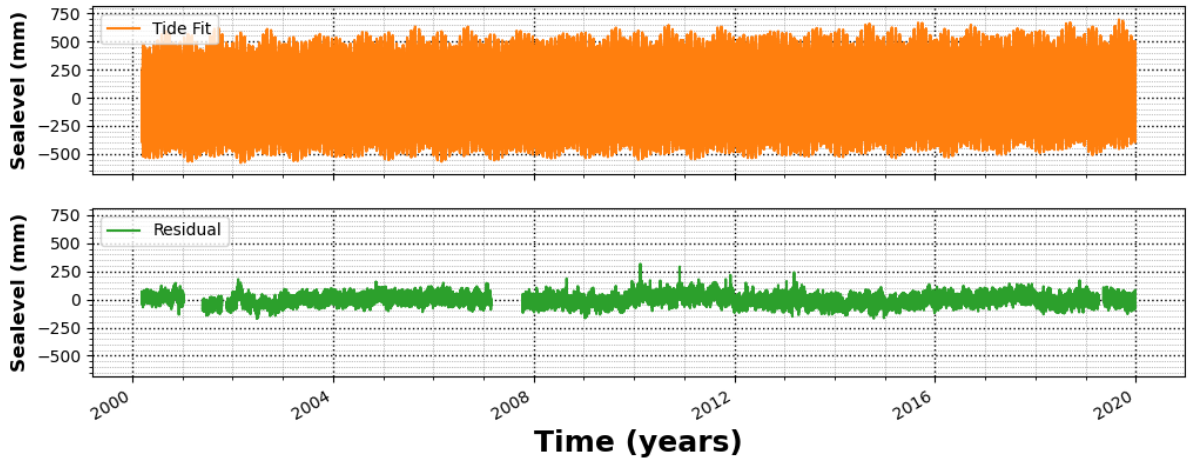

Figure 6: Times series of sea level from the tide gauge at Palmeira, Sal. Orange (Tides from UTide package) and Green (Residue). Gaps are periods of no records in tide gauge data.

To further compare the tidal analysis on the observational data we used the TPXO tidal model based on Egbert and Erofeeva (2002). For the Palmeira, Sal region the TPXO first six contributing tidal constituents were similar to the UTide analysis and also the amplitude compared very well with returns of 99.7% for O1, 98% for M2 and S2 and 93% for N2, K1 and K2. The TPXO model also revealed that the average tidal range of the Cape Verde region was slightly higher for most of the constituents (Table 3). The TPXO model gives 15 constituents which makes the resultant tidal range (705mm) slightly lower as compared to the 68 tidal constituents by the UTide package. The tidal range of the Cape Verde Archipelago also decreases as one moves up the latitude.

Table 3 contains the amplitude of the all tidal constituents greater than 10mm as extracted using UTide and the amplitudes as deduced from the TPXO model (Palmeira and the Cape Verde). Empty sections under the TPXO model amplitudes are due to no results by the model for such tidal constituents.

Table 3: Tidal Constituents and their amplitudes as extracted by UTide python package from the tide gauge at Palmeira, Sal and that deduced by the TPXO model for the tide gauge location in Palmeira and for the whole Cape Verde region.

Constituents #	Name	UTide Amplitude (mm)	TPXO Amplitude (mm) Palmeira	TPXO Amplitude (mm) Cape Verde	Period (Hours)
1	M2	304.0183831	298.5330522	332.172650	12.42
2	S2	117.7895335	115.2189672	119.106587	12
3	N2	60.13022299	55.55750802	65.107388	12.66
4	K1	49.37478024	45.76972499	46.306342	23.93
5	O1	39.17943764	39.30375725	38.570771	25.82
6	K2	31.46138153	33.77472237	33.987464	11.97
7	SA	29.5072882	-	-	365.26

8	SSA	16.92913434	-	-	182.63
9	P1	15.94333903	12.70047296	12.780584	24.07
10	MF	14.56325653	14.1701512	14.546523	13.66
11	MU2	12.01354614	-	-	-
12	Q1	11.4471512	11.65047102	11.299446	13.4
13	M4	11.34790239	8.041316643	7.641908	6.21
14	NU2	10.6159409	-	-	-

It was noted that the FFT leads to production of frequency bins of the same length as the data. The Solar Annual tide has a peak at a yearly rate and it is the tidal constituent with a large periodicity but significant contribution to the tidal regime of any location. Figure 7 shows the Solar Annual tide contribution, which has a frequency of about 365.25 days or 8800 hours. The UTide package was able to take out the SA tide as seen in the figure below as the energy level at the SA tide frequency (green dotted line) is largely taken out as seen in the residue at about an 84% success rate.

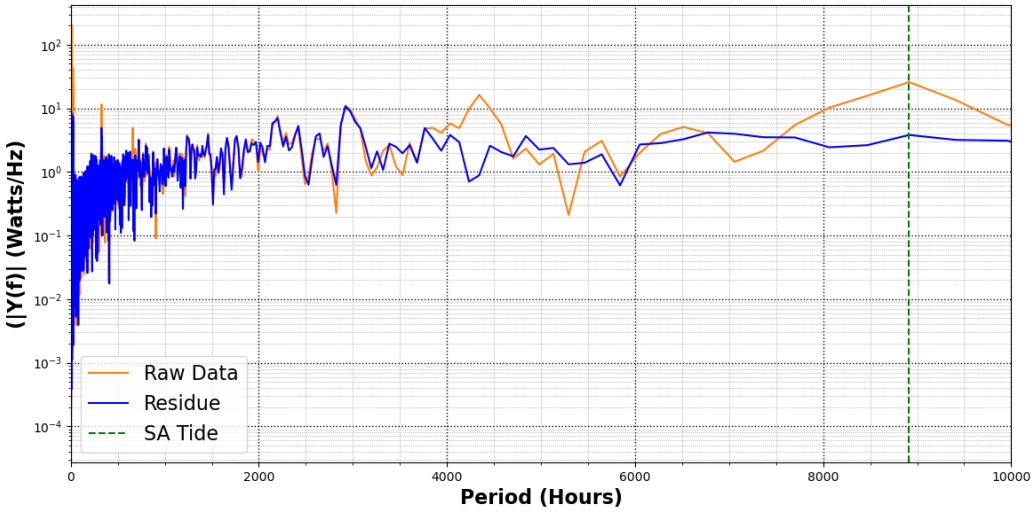

Figure 7: Spectral Analysis showing the frequency position of the Solar Annual tide (Green) and its energy level in the raw data (orange) and the residue (blue).

Looking at the SA tide's energy in the sea-level observations and the residue datasets does not give a full extent of the effectiveness of the UTide package. To better evaluate the performance of the UTide package, the energies of the highest contributing tidal constituents from Table 3 needs to be analyzed in the sea-level observations and residue datasets. It is worth noting that most tidal constituents have their peaks under two weeks (336 hours). In the case of this study, the highest contributing tides Principal Lunar (M2), Principal Solar (S2), Larger Lunar Elliptic (N2), Luni-Solar Diurnal (K1), Principal Lunar Diurnal (O1) and Luni-Solar Semidiurnal (K2) all have periods under 27 hours (António & Machado, 2017). Due to

this, to gain an understanding into the effectiveness of the UTide Python package, the single-sided power spectrum plot was zoomed into 10 to 30 hours (Figure 8). The results showed the energies of the six highest contributing tides were significantly reduced when the UTide package was used for the extraction with a performance of about 96% for the Principal Solar (S2) tide signal as seen in Figure 8.

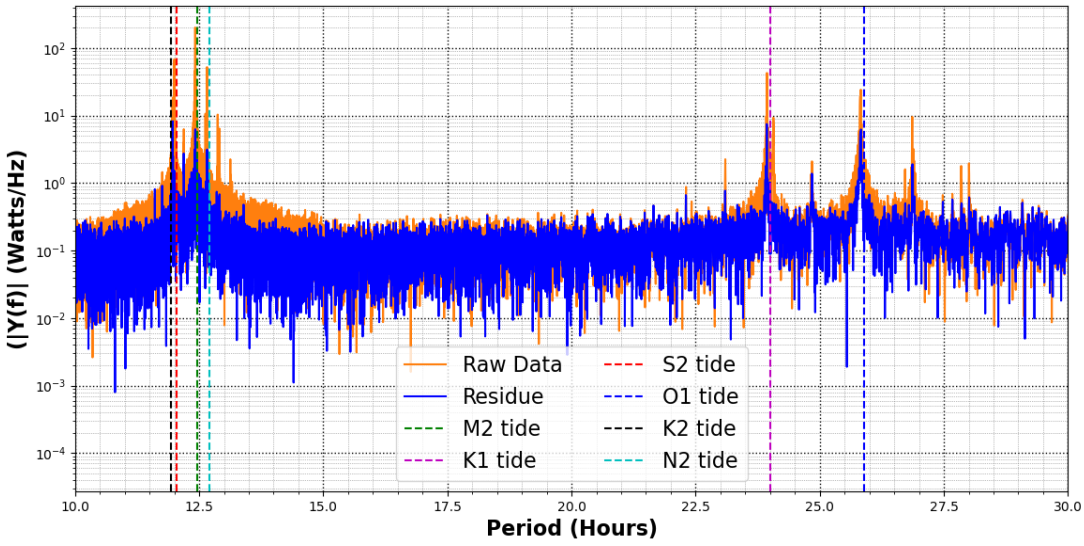

Figure 8: Spectral Analysis showing the energy of the top 6 tides before (orange) and after (blue) using the UTide package. Tidal constituents marking from left to right, K2 (black), S2 (red), M2 (green), N2 (cyan), K1 (magenta) and O1 (blue).

4.3 Surges and Extreme Lows induced Sea-level Variability

By subtracting the tidal signal as determined by UTide from the sea-level observations data a time series is obtained that now is further investigated for potential drivers.

For the surges and extreme low, our interest is in short term variability, hence we applied a high pass (signal <14 days) filtering to the time series that has the tides removed (Figure 6 bottom). The high pass filtered residual time series (Figure 9) shows a number of extreme high and low events that eventually are associated with surges (name used here for "high events"). Surges were more prevalent between 2008 and 2014 whiles the extreme low events were all but two in 2013 and 2014. A total of 12 extreme low events (Table 4) and 37 surges (Table 5) were observed, that is there were 37 instances in time were the sea-level was greater than four times the standard deviation (114.86mm) and 12 instances in time when it was less than (-114.86mm). No surge or extreme low was observed during the period of Hurricane Fred (August 2015) (Figure 6, red rectangle).

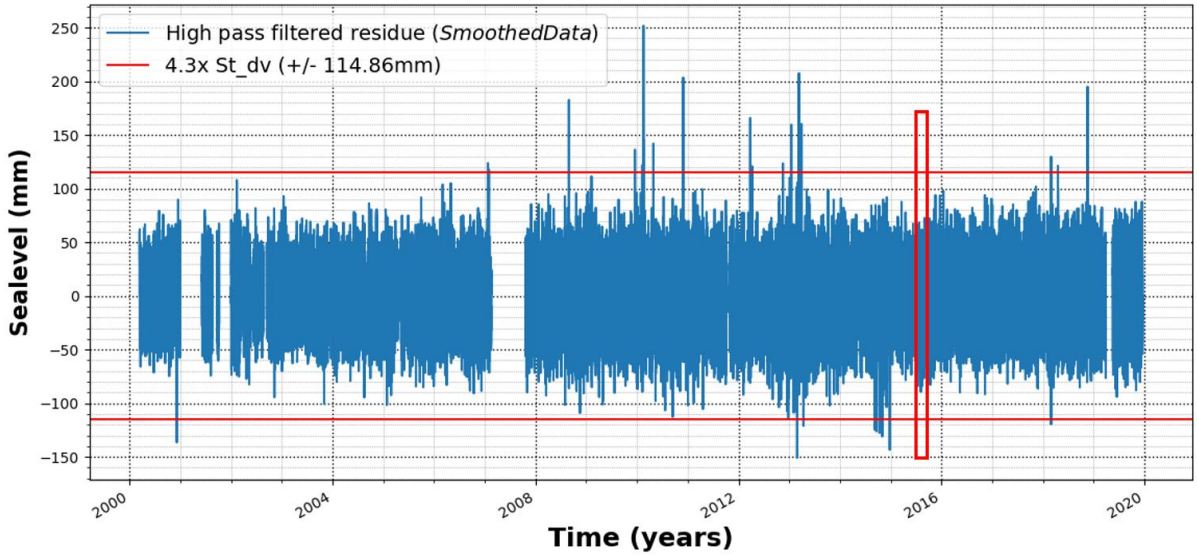

Figure 9: High path filtered (14 days) residual (tides removed) times series. Red lines represent 4.3x of standard deviation. Any moment where the blue lines cross the red lines is termed as a strong event. Red rectangle is period of Hurricane Fred (August 2015).

Table 4: Extreme Low events (moments where the sea level was less than -4.3x the standard deviation) identified and water level at the noted times.

Time (m/d/y hour)	Water level (mm)
12/5/2000 6:00	-136.4624438
2/26/2013 10:00	-150.8510694
2/26/2013 11:00	-129.4825419
4/13/2013 2:00	-121.1230999
9/8/2014 23:00	-124.7129985
9/19/2014 22:00	-126.1325893

Time (m/d/y hour)	Water level (mm)
10/12/2014 1:00	-117.7335287
10/12/2014 2:00	-127.5978809
11/1/2014 0:00	-130.9551065
12/25/2014 3:00	-127.8016549
12/25/2014 4:00	-143.3889755
2/28/2018 19:00	-119.6184154

Table 5: Surges (High events) (moments where the sea level was more than 4.3x the standard deviation) identified and the water level at the said times.

Time (m/d/y hour)	Water level (mm)
1/23/2007 5:00	123.8639659
1/31/2007 3:00	117.561976
8/27/2008 23:00	168.0011549
8/28/2008 0:00	182.6925182
8/28/2008 1:00	126.324483
8/28/2008 3:00	130.121663
12/16/2009 21:00	136.3281098
2/8/2010 13:00	122.0244859
2/15/2010 0:00	145.9143157
2/15/2010 21:00	251.8683544
2/15/2010 22:00	163.5549028
4/28/2010 8:00	142.0999114

Time (m/d/y hour)	Water level (mm)
11/16/2012 1:00	123.5993395
1/15/2013 10:00	159.6758735
3/10/2013 19:00	120.5949598
3/10/2013 20:00	187.0008443
3/10/2013 21:00	171.3048364
3/10/2013 22:00	156.7643847
3/10/2013 23:00	181.4676232
3/11/2013 9:00	207.6342917
3/11/2013 10:00	202.968457
3/11/2013 21:00	121.5803146
3/30/2013 11:00	158.2296063
3/30/2013 12:00	160.3668421

11/29/2010 1:00	203.5628629		2/28/2018 20:00	126.4484276
11/29/2010 2:00	162.583329		2/28/2018 22:00	129.7958576
11/29/2010 3:00	136.4905168		4/18/2018 23:00	121.3234715
11/29/2010 4:00	145.029737		11/18/2018 19:00	169.5939465
3/25/2012 11:00	165.8740986		11/18/2018 20:00	195.0101481
3/25/2012 12:00	120.466701		11/19/2018 6:00	184.9089591
4/8/2012 10:00	120.8592375			

4.3.1 Surges and Extreme Lows in Relation to Wind and Surface Waves

Our interest is to understand the drivers of the extreme (high or low) events. One potential driver could be local wind events that drive a pile of water at the site. However, we see a weak correlation between the wind speed and direction with the high pass filtered residue sea level data used for the events identification (Figure 9). The correlation between the wind speed (wind direction) and high pass filtered data was -0.08 (0.04) and not significant.

The high pass filtered residue sea level data when compared with the surface waves data of the Palmeira area (tide gauge region) and high pass filtered significant wave height of surface waves data yielded -0.04 correlations in both instances. Table 6 gives insight into the SWH of surface waves and wind conditions during the times of the surges (positive water level values) and extreme lows (negative water values).

Table 6: SWH and wind conditions during the times of the strong events both high(+ Water level values) and low (-Water level values).

Time (m/d/y hour)	Water level (mm)	Wind_Speed (m/s)	Wind_Dir	SWH (mm)
11/19/2018 6:00	184.9828646	9.516722679	45.07426453	3342.499971
11/18/2018 20:00	195.0865832	7.548559189	39.67312622	3182.499886
11/18/2018 19:00	169.6706064	7.414014339	38.83105469	3159.999847
4/18/2018 23:00	121.2833869	6.91299057	54.66256714	2604.166508
2/28/2018 22:00	129.8163036	7.27439785	57.75613403	3240.833282
2/28/2018 20:00	126.4675762	7.614778996	58.69541168	3279.166698
2/28/2018 19:00	-119.5999175	7.740531921	57.19139862	3235.833406
12/25/2014 4:00	-143.3997324	8.086091995	74.43852234	1021.666646
12/25/2014 3:00	-127.8117486	7.860980511	74.96625519	1019.999981
11/1/2014 0:00	-131.0289878	9.113670349	63.45450592	1075.000048
10/12/2014 2:00	-127.5218833	6.150653839	46.5224762	1639.166594
10/12/2014 1:00	-117.6577707	6.157628059	48.18363953	1635.833263
9/19/2014 22:00	-126.1303069	5.044018269	106.2387848	1591.666619

9/8/2014 23:00	-124.6469302	4.911950588	73.06266022	1459.999959
4/13/2013 2:00	-121.1243694	6.559283733	68.77846527	1931.666652
3/30/2013 12:00	160.3319948	8.025758743	66.54064941	2295.000076
3/30/2013 11:00	158.1953644	7.896753311	66.89961243	2301.666737
3/11/2013 21:00	121.5726925	7.410443783	64.39789581	2409.999847
3/11/2013 10:00	202.9535512	7.871045113	60.52184296	2734.166622
3/11/2013 9:00	207.6187289	7.805933475	64.04735565	2769.999981
3/10/2013 23:00	181.4455557	7.577548027	62.65735626	3028.333187
3/10/2013 22:00	156.7416742	7.908150196	65.19646454	3039.166451
3/10/2013 21:00	171.2814845	8.12739563	67.1545105	3049.999714
3/10/2013 20:00	186.9768525	8.200366974	68.38592529	3047.499816
3/10/2013 19:00	120.5703297	8.110825539	72.58425903	3044.999917
2/26/2013 11:00	-129.5140224	5.512495041	76.12483215	1973.333399
2/26/2013 10:00	-150.8819323	5.904240131	79.71323395	1949.166735
1/15/2013 10:00	159.7570382	9.079491615	61.65494537	2620.833238
11/16/2012 1:00	123.6668861	9.008152008	48.61997986	1808.333238
4/8/2012 10:00	120.9159341	7.837738514	49.67637634	1546.666662
3/25/2012 12:00	120.4366202	7.64677906	47.4455719	2642.499924
3/25/2012 11:00	165.8433974	7.633003712	45.24830627	2637.499889
11/29/2010 4:00	144.9496835	7.661054134	51.62200928	1787.499944
11/29/2010 3:00	136.4103505	8.079282761	53.78778076	1752.499938
11/29/2010 2:00	162.5030554	8.193344116	54.14504242	1698.333303
11/29/2010 1:00	203.4824873	8.305703163	54.40702057	1644.166668
4/28/2010 8:00	142.1123148	4.198166847	31.80938721	1915.833235
2/15/2010 22:00	163.4750128	8.215725899	72.81439972	2397.499879
2/15/2010 21:00	251.7883442	8.29345417	74.32326508	2422.499895
2/15/2010 0:00	145.8330419	8.938628197	72.71338654	1657.500029
2/8/2010 13:00	122.000546	7.028558731	54.41889191	3152.499994
12/16/2009 21:00	136.2656782	2.813314199	63.53928375	2272.4998
8/28/2008 3:00	130.0761888	6.949866772	69.28905487	1335.000038
8/28/2008 1:00	126.2779063	6.449834347	69.58332825	1359.999975
8/28/2008 0:00	182.6453949	6.045783997	65.89253998	1372.499943
8/27/2008 23:00	167.9534883	5.834970474	59.40682983	1350.833257
1/31/2007 3:00	117.490878	8.558039665	55.03153229	2359.999895
1/23/2007 5:00	123.8240793	6.576576233	66.75523376	1616.666635
12/5/2000 6:00	-136.3914546	7.481426239	29.41850281	2642.499924

4.4 Waves induced Sea-level Variability

The significant wave height of surface waves of Palmeira, Sal Island had a temporal variability that was significantly close to that of the whole Cape Verde with a correlation of 0.974. The SWH was averagely about 1,7000mm (1.7 meters) during study period but had moments where the SWH was more than twice the average conditions and showed some level of seasonality as seen in Figure 10.

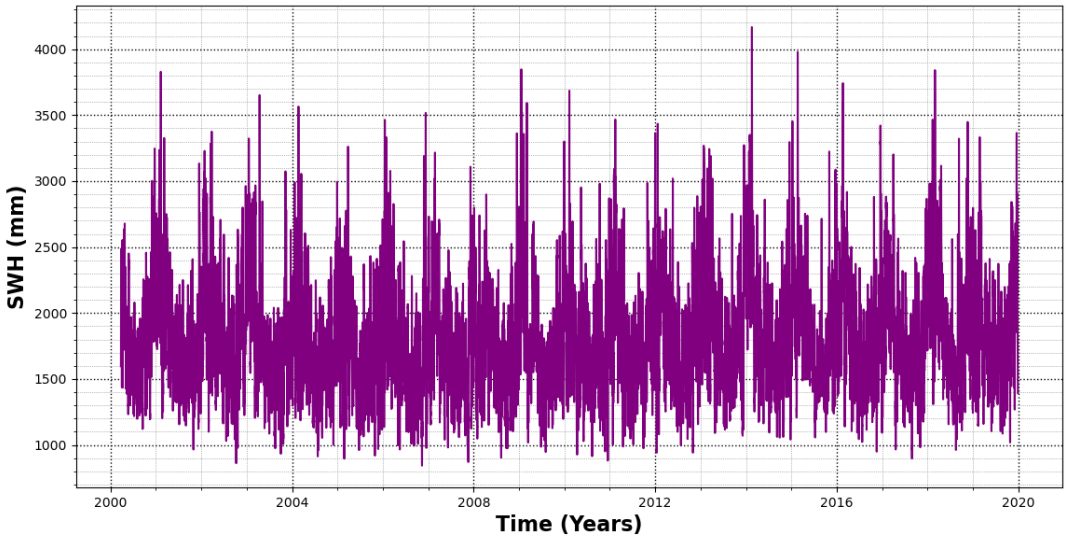

Figure 10: Temporal Variability of Significant Wave Height (SWH) of surface waves for Cape Verde.

The seasonal cycle revealed the SWH of surface waves of Cape Verde and Palmeira was highest in February and lowest in August (Figure 11). Thus, the SWH intensifies between August (first month) to its highest point in February (second month) and vice versa. The Cape Verde wind forcing during the study period also showed similar seasonality (Figure 11).

During the study period, the waves were highest in the Northern part, more than 2,000mm (2meters) in height while it ranged between 1,450 to 1,560mm within the islands (Figure 12). The waves also tend to reduce in height as it approaches the coast and the orientation of the wave height contours gives an indication that the waves originated from the North. The wave direction is affirmed in Figure 13 as the wave rose indicates that, the waves around the islands were predominantly from the North East and North-North East.

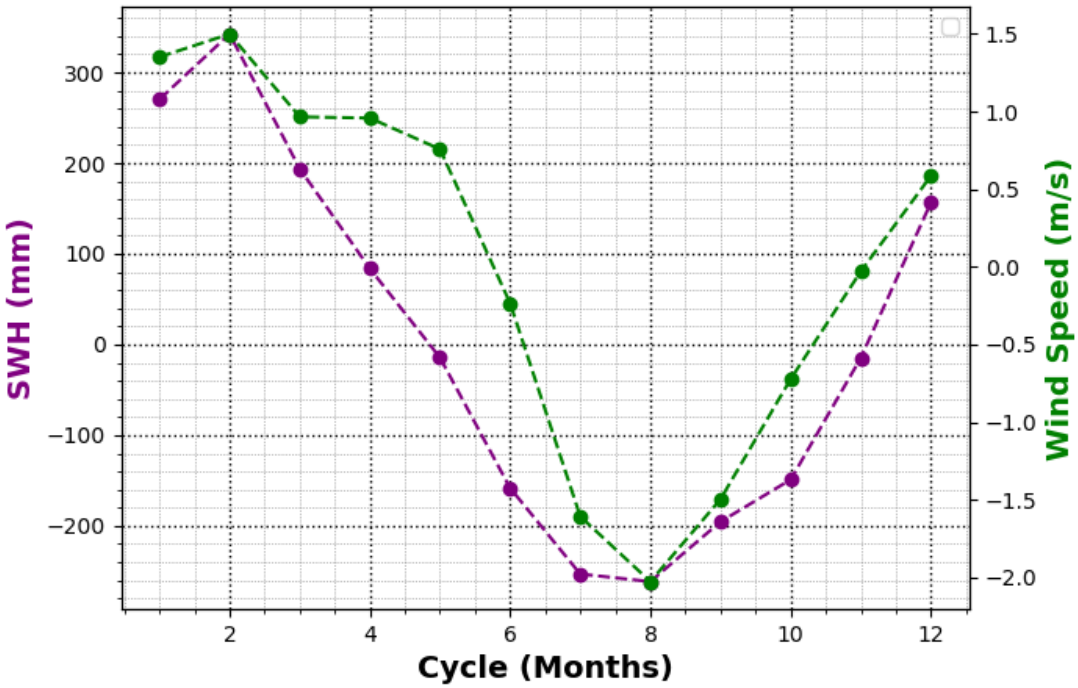

Figure 11: Seasonal cycle by month of significant wave height (SWH) (magenta) and wind (green) of the Cape Verde region during the study period.

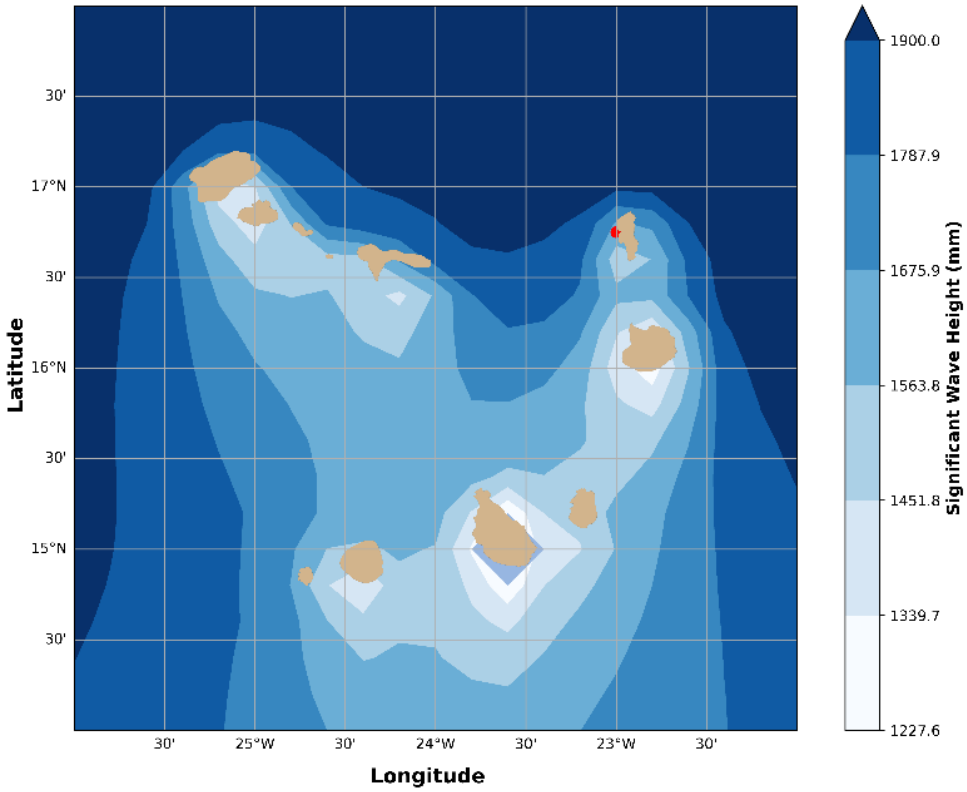

Figure 12: Spatial Variability of significant wave height during the study period. Highest to the north of the northern islands and lowest along the coast.

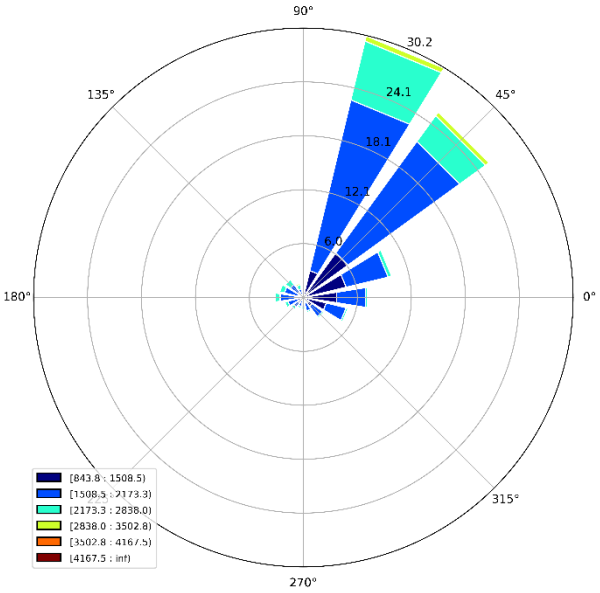

Figure 13: Wave rose indicating the predonimantly North East and North-North East (35°-75°) direction of the waves in Cape Verde.The area is dominated by waves of height between 1500 and 2200mm. 0° is East, 90° is North and so on.

If one was to visit the beach on any day during the study period, the probable SWH one might observe would be between 1,500mm while the wave direction would likely be 35 to 75 degrees with a period between 7 to 10 seconds. If only waves greater than 2,500mm are considered, the waves from the South East (270 to 350 degrees) (Figure 14; right) becomes more prominent and the periodicity will most likely slightly reduce (Figure 15).

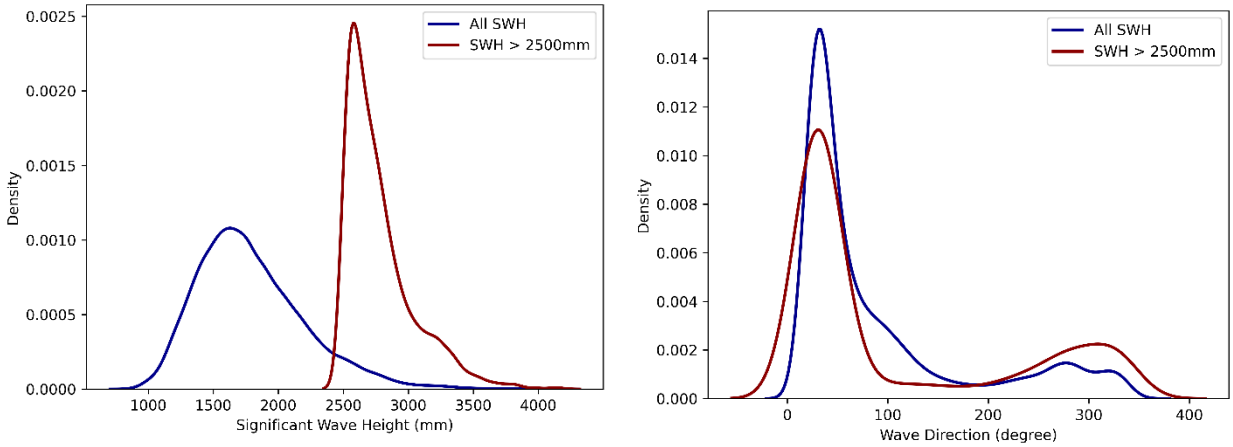

Figure 14: Probability Density Function of SWH (left) in Cape Verde. All SWH used (blue), only SWH above 2500mm (red). PDF of Wave Direction (right) in Cape Verde. All SWH used (blue), only SWH above 2500mm (red).

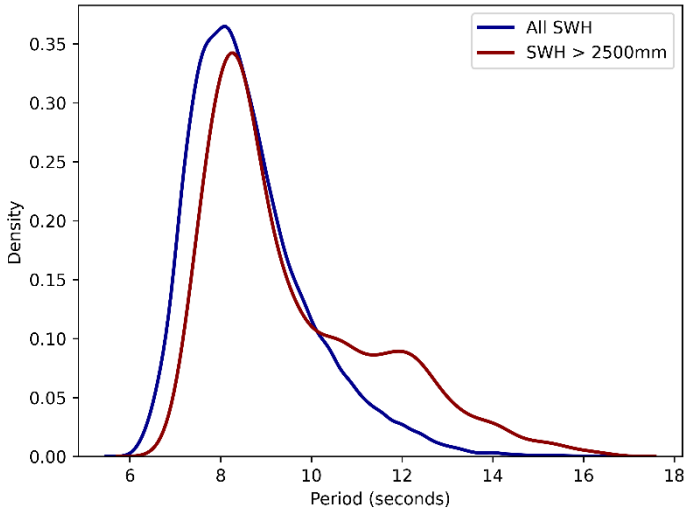

Figure 15: Probabilty Density Function of Wave Period in Cape Verde. All SWH used (blue), only SWH above 2500mm (red).

4.5 Satellite based dynamical heights Sea-Level Anomalies

The residual sea level range for Palmeira as deduced from the tide gauge was 212mm, 208mm for the reanalysis dataset and 182mm for the satellite dataset. The sea level range of the entire Cape Verde was 143mm for the reanalysis dataset and 145mm for the satellite (Figure 16) which is comparatively lower compared to that of Palmeira. The correlation result showed low correlations of 0.4 between the tide gauge and reanalysis and satellite data for Palmeira. The correlation between the satellite for Palmeira and Cape Verde as well as reanalysis dataset between the locations were 0.9 and 0.87 respectively.

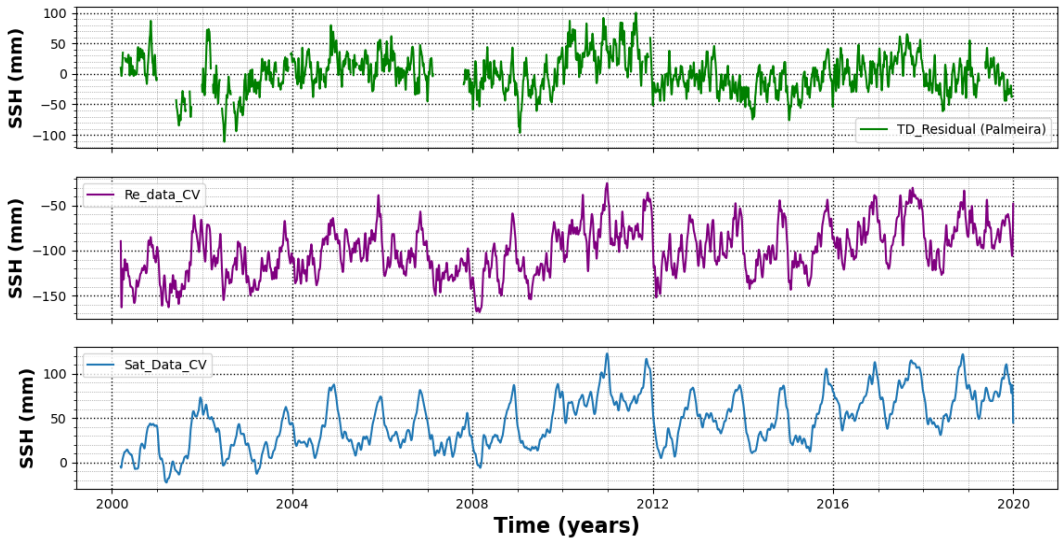

Figure 16: Sea level of Cape Verde during the study period. From top to bottom: [Tide Guage residual (TD_Residual (Palmeira; green), Reanalysis for Cape Verde (Re_data_CV; magenta), Satellite Cape Verde (Sat_data_CV; blue)].

The three kinds of events identified in the time series where there was a sudden change in sea level were;

i. High in both the model and tide gauge (December 11, 2011 to January 10, 2012).
ii. High in the model but low in tide gauge (November 1, 2003 to December 17, 2003).
iii. Low in the model but high in tide gauge (November 9, 2000 to December 3, 2000).

The event (i) is so because the change in sea level during the event is similar across all the Cape Verde islands (Figure 17 left). During the event (ii) as the Palmeira area (red dot) had a significant change in sea level while most part of the Cape Verde comparatively smaller changes in sea level (Figure 17 right). The reverse is observed in event (iii) as there is a significant drop in sea level at Palmeira (red dot) while most part of the Cape Verde witnessed an increase of sea level (Figure 18).

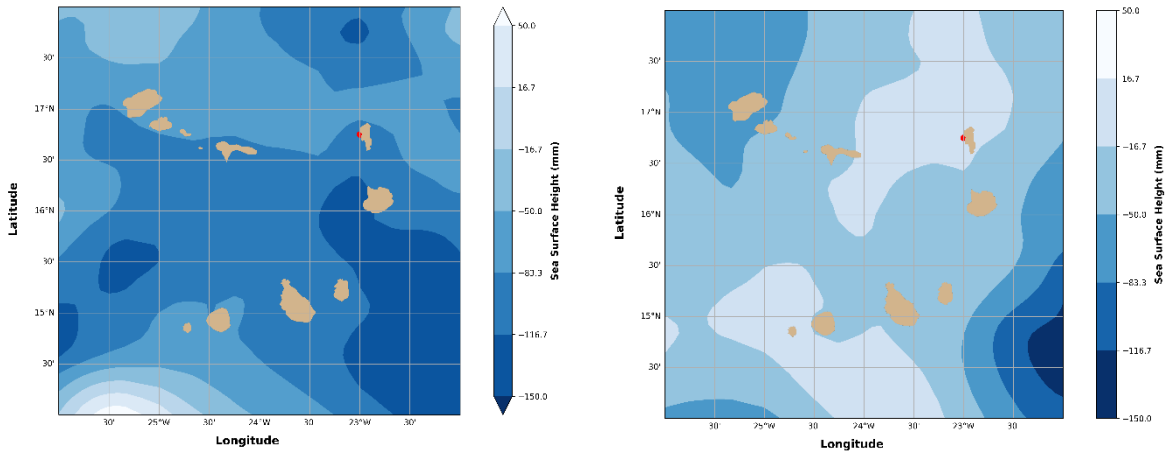

Figure 17: Sea level variability in Cape Verde during event type i (right) and event ii (left) as seen in the text. Darker colors represents a drop in the sea level and brighter colors an increase in sea level during the event.

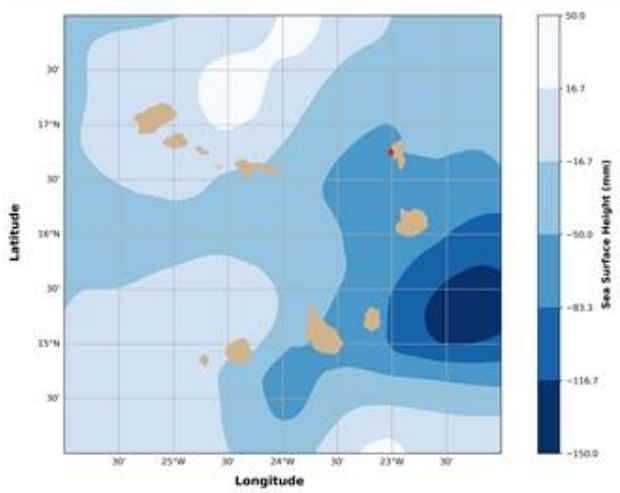

Figure 18: Sea level variability in Cape Verde during event type (iii) as seen in the text. Darker colors represents a drop in the sea level and brighter colors an increase in sea level during the event.

There was an upward trend in the sea level for the satellite and reanalysis datasets while a slightly downward trend was observed in the tide gauge dataset (Table 7). The rate of increase of sea level was found to be highest in the satellite dataset as compared to the reanalysis dataset (Table 7).

Table 7: Rate of change of sea level using the various datasets for the study period.

Data_Type	Sea level change (mm/year)	Standard Error (mm/year)
Tide_Guage	-0.156	0
Palmeira_reanalysis	2.106	3.77×10^{-10}
Palmeira_satellite	3.174	1.39×10^{-9}
Cape Verde_reanalysis	2.238	0
Cape Verde_satellite	3.024	7.65×10^{-10}

The seasonality by month deduced from the datasets were slightly varying but it showed November had the highest sea level during the study period in all the datasets except the tide gauge (Figure 19). There is a rise in sea level from July and peaks in November and starts to declines sharply after.

The sea level of Cape Verde independent of the tides showed a good correlation with the local wind stress curl (0.62) and the sea surface temperature (0.70) (Figure 20). The sea level showed a delayed response to the wind stress curl and the sea surface temperature as these conditions peaks in the later months of the year.

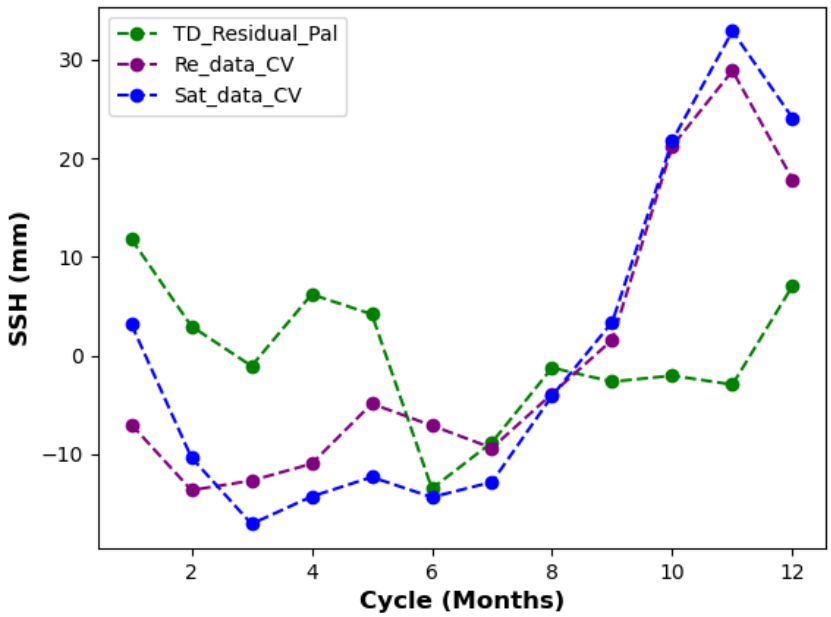

Figure 19: Seasonlality by month of Sea level of Cape Verde. [Tide Guage Residual of Palmeira (green), Reanalysis for Cape Verde (Re_data_CV; magenta, Satellite Cape Verde (Sat_data_CV; blue]

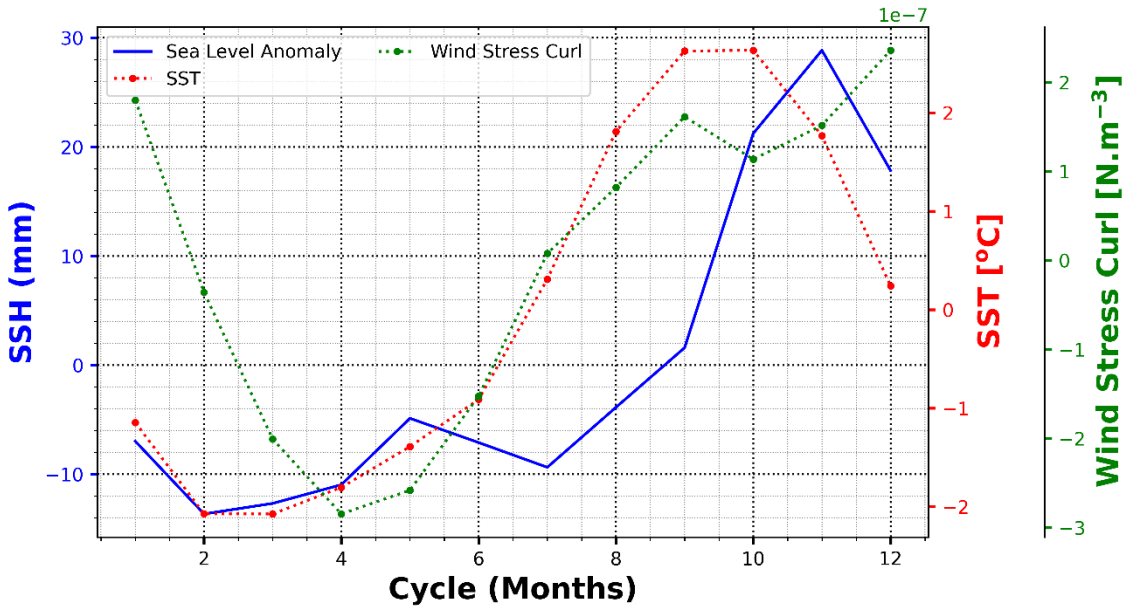

Figure 20: Seasonal cycle by month of Sea level in Cape Verde and how its changes with the region's Wind stress Curl and Sea Surface Temperature.

5. Discussion

5.1 Tidal Contribution

The tidal range of Palmeira, Sal was found to be 815mm as deduced from UTide with the principal lunar semidiurnal tide (M2) accounting for most with an amplitude of 304mm which agrees well with the findings of Le Provost et al., (1995) and Gerkema (2019) having computed the range of the global ocean considering the amphidromic points of the M2 tides. Using the same approach, Gerkama (2019) indicates the expected the luni-solar declinational diurnal component (K1) tidal range for the Cape Verde (Sal) should be similar to what was attained from the analysis of this work (about 49mm). The tidal range for the Cape Verde region was found to be 705mm but this could be explained by the reduced number of tidal constituents the model provides rather the whole region being less than that of Palmeira. Due to the closely related values from the TPXO model for the Cape Verde region to that of Palmiera, we can say that the range deduced from UTide analysis (using the tide gauge data) is a good representative of the whole Cape Verde region's tidal range. The tidal constituents as per the tide gauge data was affirmed by the TPXO model results (Table 3) for Palmeira with over 93% accuracy for the top six tides and their amplitudes and 98% accuracy for the two top tides (M2 and S2). Gomes et al (2015) also found the same top six tidal constituents by using MATLAB's T_Tide package by Pawlowicz et al. (2002) for the tide gauge data in Palmeira. The amplitudes found by Gomes et al (2015) was also 95% of what was found in this study for the top six tidal constituents. The spectral analysis carried out (Figure 7 & 8) also revealed that the UTide package was effective in removing the tidal signals to a high degree and the UTide package by Codiga (2011) can be said to be an effective tool in extracting the tides from a tide gauge data. The six highest contributing tides are all tidal constituents with less than 27 hours periodicity with M2 and S2 having 12.42 and 12 hours periodicities respectively (António & Machado, 2017). Thus the Palmeira coast has close to 815mm variability in the coastal sea level if most of the tidal constituents were to occur at the same moment.

5.2 Surges and Extreme low Contribution

The isolated 49 moments of surges and extreme low sea levels (+/- 114.86mm) from the tide gauge (Figure 9) did not show any pattern with the local wind or waves (Table 6). No particular month also showed dominance in either the surges or extreme low events. However

10 of the 12 extreme low events were between 2013 and 2014. What could have occurred in those two years to create those kind of conditions? The highest surge of Palmeira was 251.8mm (Table 6) which is just 15% and 10% of the maximum surge recorded in Naples, Florida (1600mm) and Fernanadina Beach (2400mm) during Hurricane Irma in Septemnber, 2017 (Sangdon et al., 2019). However there was no record of surges or extreme lows in the tide gauge data at Palmeira during Hurricane Fred. Hurricane Fred occurred in August 2015 and affected 7 of the 10 Islands (Jenkins et al., 2018) including Sal Island, where the tide gauge is located. There was however no direct strike on any island observed in the track of the hurricane (Jenkins et al., 2018). There should be a proper monitoring system of tropical cyclone (TC) genesis in other to provide early warning systems as climate change and warmer sea surface temperature may lead to rapid intensification of TC (Villarini and Vecchi, 2013). This would make Cape Verde more prone to being hit by a hurricane and storm surge as the hurricanes' landfall could occur early in the Atlantic rather than travelling to the Caribbean and North America region.

114.86mm and above for the surges might seem insignificant when compared to the tidal (815mm) and surface wave (averagely 1,700mm) ranges. But if a surge occurs at a time of the highest high tide and highest wave, it could easily overtop coastal defense structures that did not factor in the contribution of the surges. Extreme low events occurring during low tides could also impact local desalination plants by limiting available water. The documentation on surges if any for the Cape Verde is poor and needs to be studied deeply as surges are expected to increase due to the effects of climate change (World Bank Group, 2015).

5.3 Waves Contribution

The SWH of Cape Verde (Figure 10) indicates that the Cape Verde sea level variability has its highest contribution coming from waves with wave heights varying around 1,700mm (1,000 to 4,400mm). Wave heights of such magnitudes are considered suitable for wave power generation, making Cape Verde a suitable zone for wave power plants. One other reason of the area being suitable for wave power generation is the non-existence of excessively strong or high waves, the highest during the study period being about 4,400mm unlike the 14,000 to 25,000mm of the Azores (Bernardino et al., 2017) because excessively strong waves can destroy the wave power plant system put in place. Mørk et al., (2010) documents clearly the suitability of the Cape Verde region for wave power (15-20kW/m) generation. The northern coastal zones of the north islands (Santo Antoa, Sao Vicente, Sao

Nicolau, Santa Luzia and Sal) could be more resourceful for wave power generation. This is due to the waves of Cape Verde originating mainly from the North East and North-North East direction (Figure 13). The north islands, tend to act like a shelter and reduce the SWH as the waves come into contact with the land mass (Figure 12), making the northern coast of the north islands to have higher SWH than the rest of the Cape Verde Islands.

The waves of the area tend to have similar wave direction if all wave heights are considered and if only waves greater than 2,500mm are considered (Figure 14; right) with slightly delayed wave periods (Figure 15) for higher wave heights. The areas wave heights monthly seasonal cycle (Figure 11) had the same fluctuations as the local wind speeds monthly cycle (Figure 11) and this is explained by waves being generated by wind speeds blowing over a distance (fetch) for a period of time. Cape Verde is surrounded by the ocean and with winds coming from the North East, it creates conditions for the higher wind speeds to have a large fetch with little to no obstruction and these makes it suitable to generate higher waves.

5.4 Satellite based dynamical heights Sea level anomalies of Cape Verde

The sea level anomaly range for Palmeira as deduced from the CMEMS sea surface height reanalysis data (208mm) was 98% that generated from the tide gauge (212mm) while the CMEMS sea level anomaly satellite data (182mm) was 86% as compared to the tide gauge. However the behavioral patterns in the CMEMS datasets had no significant relation to that of the tide gauge with 0.4 correlation (Figure 16, 19). Prandi et al. (2009) points out how tide gauges exhibit more variability as compared to satellite data having used data from 91 gauges from the University of Hawaii Sea Level Center (UHSLC). Coastal features such as the continental shelf can make coastal sea level variability different from the adjacent open ocean (Woodworth et al., 2019). The daily sea level anomalies of Palmeira were in close synchronize with that of Cape Verde when using the CMEMS reanalysis or satellite dataset.

The observed Palmeira sea level trend in the tide gauge (-0.156mm/year) was not consistent with what is provided by the reanalysis (2.1mm/year) or satellite (3.2mm/year) dataset (Table 7). However, the observed trend agrees with findings (-0.15 ± 0.28mm/year) of Mendes et al., (2017) when a discontinuity (due to change in hardware) is introduced in the dataset. Thompson et al. (2016) found that <1% of tide gauge sea level trends tend to match the global reported trends for the twentieth century and points to poor siting of these gauges as the reason. This could be a reason for the difference in observed trend from the tide gauge and

that of the model reanalysis and satellite observation as the tide gauge is located in a semi-enclosed bay, a similar situation is reported near the coast of Benguela (Habib et al., 2019). Also, due to the Cape Verde being a volcanic island, there is the likely influence of tectono-volcanic mechanisms in its geodynamic setting which could influence sea level trends from tide gauges as a result of vertical land motion (-1.06mm/year) (Mendes et al., 2017). Geological records of Sal indicates an uplift of the island over time (Torres et al., 2002; Zazo et al., 2007). The local changes in sea level trend at Palmeira is closely linked to that of the whole Cape Verde with 2.2mm/year and 3.0mm/year for reanalysis and the satellite respectively. The sea level trend in Cape Verde using the satellite data (3.02mm/year) during the study period (2000 to 2019) compares well with the global sea level rise (2.88 to 3.61mm/year) for 1993 to 2018 (Oppenheimer et al., 2019) captured in the 2021 Intergovernmental Panel on Climate Change (IPCC) report. Thus, during the study period, Cape Verde was witnessing a sea level rise similar to that of global average.

Sea level seasonality is said to have a variety of forcing mechanisms including winds (Woodworth et al., 2019). This was found to be valid for the study area as the monthly seasonality in sea level variability in Cape Verde is closely associated to the regions wind stress curl and sea surface temperature (Figure 20) similar to the findings of Akhter et al. (2021) for the northern Bay of Bengal in the Indian Ocean.

7. Conclusions

i. How large is the sea-level variability induced by tidal currents based on a local analysis for the Cape Verde Islands?

Answer: The tides contribute about 815mm to the sea level variability of Cape Verde and it is the second highest contributor. M2 tide being the dominating tidal constituent.

ii. How large is the sea-level variability induced by surface waves based on a regional analysis for the Cape Verde Islands?

Answer: The waves contribute about 1,700mm on an average to sea level variability of the Cape Verde. However, the range of waves vary from 1,000 to 4,400mm with periods of less than 12seconds. The winds is a driver of the seasonality of the area's waves.

iii. How large is the regional and large scale sea-level variability induced by changes in dynamic topography for the Cape Verde Islands?

Answer: Changes in dynamic topography contributes 182 to 212mm to the large scale sea-level variability of the Cape Verde and it is at its highest in November with strong ties to the SST and wind stress curl.

iv. Which recommendations can be given for coastal management for the Cape Verde region related to sea-level variability based on the results?

Answer: In probing into the sea level anomaly, it was observed that the location of the tide gauge in Palmeira (in a bay) could be the primary cause in not giving a good representation of the sea level anomalies as compared to the satellite or modelled data. The unavailability of tide gauges in the area is also one hindering factor in monitoring coastal sea level conditions of the area, as there is only one tide gauge among 10 islands. Installation of tide gauges by taking into account the location will go a long way to help study the conditions of all the islands and the sea level variability of Cape Verde. Understanding these conditions will help to plan for possible coastal defense systems that would help mitigate disasters if an island is to take a hit. Coastal manager must take into account not only the tides and waves but also the possibility of surges in other not to build defense systems that are easily toppled. High resolution coastal modelling of the bay conditions (like the CMEMS works on the Mediterranean Sea) needed due to unexplained cause of surges and extreme lows.

Figure 21 summarizes the average contribution of the various drivers investigated (waves, tides, dynamic topography and surges).

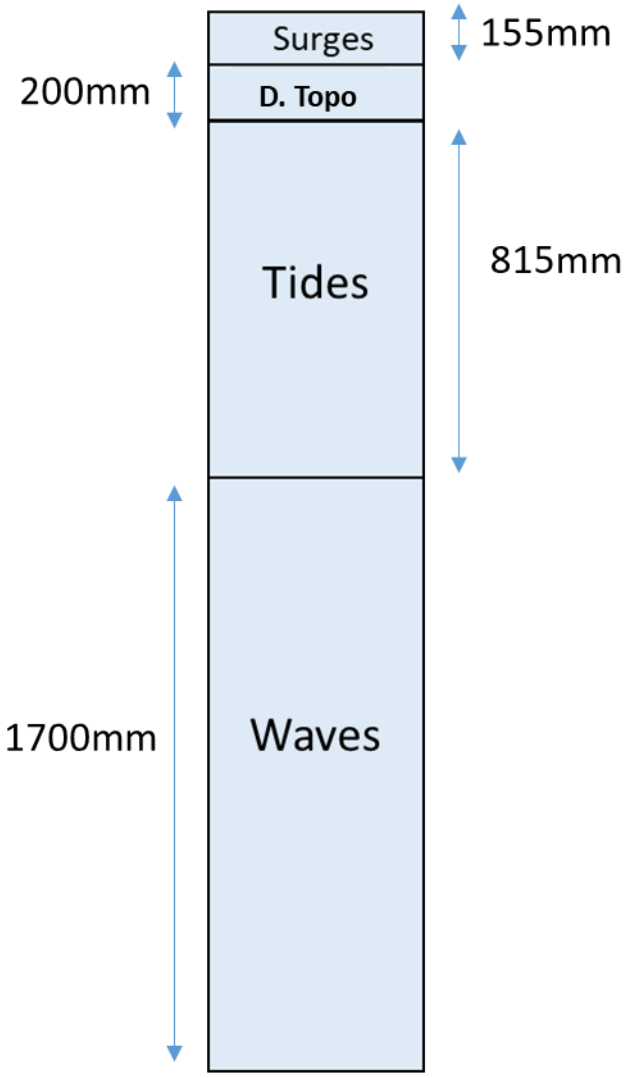

Figure 21: Pictorial Representation of the average magnitude of the contributing factors to the Cape Verde Coastal Sea Level. This is a representaion of what the situation will be at a point in time where the these events have their peaks or averages coinciding with each other. It is possible to have a surge event occuring at a point of low tide which would imply low water levels despite the surge.

8. Future Direction

Due tectonic and volcanic activities, other researchers have noted that the area undergoes vertical land motion not consistent with that of the major continents. An assessment of this and the sea level trend and how it works in tandem could help understand the level of risk the archipelago faces.

The satellite and reanalysis product for CMEMS gives a rough resolution (0.25degrees) compared to the products for the Mediterranean Sea (0.042). Thus modelling the ocean physical conditions around Cape Verde to achieve a higher resolution in other to gain detailed understanding of the area as well as the individual islands is one that could be looked at.

The country is encompassed by the ocean, but finding adequate papers on works carried out on the nation's physical oceanographic parameters is difficult. This work among others revealed the waves of the area and lack of extreme waves makes it conducive for wave power plants but it an area where there is little reported investment of funds into tapping this power source. A look at possible locations of siting wave power plants considering factors such as bathymetry, wave heights, wave period and wave power plant financial sustainability could go a long way to help support the country's electric power system.

9. References

Abdalla, S. Are Jason-2 significant wave height measurements still useful, Advances in Space Research, 2019, ISSN 0273-1177, https://doi.org/10.1016/j.asr.2019.08.032.

Abe, K. 1979 Size of great earthquakes of 1837–1974 inferred from tsunami data. Journal of Geophysical Research, 84, 1561–1568.

Abrogueña, J.B.R., Range, P., Cruz, W., Tentia-Lagumen, M.C., Chicharo, M. Fish communities and environmental variables during dry season in Pampanga estuary (Philippines) Regional Studies in Marine Science, 34 (2020), p. 101053.

Akhter, S., Qiao F., Wu, K., Yin, X., Chowdhury, K.M.A., Chowdhury, N.UM.K., Chowdhury. Seasonal and long-term sea-level variations and their forcing factors in the northern Bay of Bengal: A statistical analysis of temperature, salinity, wind stress curl, and regional climate index data, Dynamics of Atmospheres and Oceans, Volume 95, 2021, 101239, ISSN 0377-0265, https://doi.org/10.1016/j.dynatmoce.2021.101239.

Allan, J., Komar, P., 2000. Are ocean wave heights increasing in the eastern North Pacific? EosTrans. AGU 81 (47), 566–567.

Alpers, W., Hasselmann, K., 1982. Spectral signal to clutter and thermal noise properties of ocean wave imaging synthetic aperture radars. Int. J. Remote Sens. 3, 423–446.

Angnuureng, D.B., Appeaning, Addo K., Almar, R., Dieng, H.B., 2018. Influence of sea level variability on a micro-tidal beach. Nat. Hazards 93 (3), 1611–1628. https://doi.org/10.1007/s11069-018-3370-4.

Becker, A., Ng, A.K., McEvoy, D., Mullett, J., 2018. Implications of climate change for shipping: Ports and supply chains. Wiley Interdiscip. Rev. Clim. Change 9 (2), e508.

Birol, F., Fuller, N., Lyard, F., Cancet, M., Nin˜o, F., Delebecque, C., Fleury, S., Toublanc, F., Melet, A., Saraceno, M., Le´ger, F., 2017. Coastal applications from nadir altimetry: example of the X-TRACK regional products. Adv. Space Res. 59 (4), 936 953. https://doi.org/10.1016/j.asr.2016.11.005.

Brierley, A.S., Kingsford, M.J., 2009. Impacts of climate change on marine organisms and ecosystems. Curr. Biol. 19, R602–R614.

Bourdalle, R. (2012). Global Ocean Physics Reanalysis. https://sextant.ifremer.fr/record/c0635fc4-07d3-4309-9d55-cfd3e6aa788b/. Accessed on 31-May-2021.

Caballero Ainhoa, Mulet Sandrine, Ayoub Nadia, Manso-Narvarte Ivan, Davila Xabier, Boone Christine, Toublanc Florence, Rubio Anna, 2020. Integration of HF Radar

Observations for an Enhanced Coastal Mean Dynamic Topography. Frontiers in Marine Science (7) 2296-7745. https://doi.10.3389/fmars.2020.588713.

Caldwell, P. C., M. A. Merrifield, P. R. Thompson (2015), Sea level measured by tide gauges from global oceans — the Joint Archive for Sea Level holdings (NCEI Accession 0019568), Version 5.5, NOAA National Centers for Environmental Information, Accessed on 31-December 2020. Dataset, doi:10.7289/V5V40S7W.

Carter, D.J.T., Draper, L., 1988. Has the North east atlantic become rougher? Nature 332, 494.

Casas-Prat, M., Wang, X.L., Sierra, J.P., 2014. A physical-based statistical method for Modelling ocean wave heights. Ocean Model. 73, 59–75.

Cazenave, A., Dieng, H.-B., Meyssignac, B., von Schuckmann, K., Decharme, B., & Berthier, E. (2014). The rate of sea-level rise. Nature Climate Change, 4(5), 358–361. https://doi.org/10.1038/nclimate2159

Chen, Z., He, Y., Yin, B., Qiu, Z., 2012. The significant wave height distribution retrieved from marine X-band radar images. IEEE Int. Symp. Geosci. Remote Sens.2641–2644.

Chune, S. L. (2019). Global Ocean Waves Reanalysis WAVERYS. https://sextant.ifremer.fr/record/b72f483b-3557-4e4d-ab86-4619e61e3d54/. Accessed on 31-May-2021.

Church, J.A., Gregory, J.M., White, N.J., Platten, S.M., Mitrovica, J.X., 2011. Understanding and projecting sea level change. Oceanography 24, 130–143.

Church, J.A., Clark, P.U., Cazenave, A., Gregory, J.M., Jevrejeva, S., Levermann, A., Merrifield, M.A., Milne, G.A., Nerem, R.S., Nunn, P.D., Payne, A.J., Pfeffer, W.T., Stammer, D., Unnikrishnan, A.S., 2013. Sea level change. In: Stocker, T.F., Qin, D., Plattner, G.-K., Tignor, M., Allen, S.K., Boschung, J., Nauels, A., Xia, Y., Bex, V., Midgley, P.M. (Eds.), Climate Change 2013: the Physical Science Basis, Contribution of Working Group I to the Fifth Assessment Report of the Intergovernmental Panel on Climate Change. Cambridge Univ. Press, Cambridge, UK, New York, NY, USA, pp.1137–1216.

Cipollini, P., Cromwell, D., Quartly, G.D., 1998. Observations of Rossby wave propagation in the Northeast Atlantic with TOPEX/POSEIDON altimetry. Adv. Space Res. 22 (11), 1553–1556. https://doi.org/10.1016/S0273-1177(99)00069-1.

Codiga, D.L., 2011. Unified Tidal Analysis and Prediction Using the UTide Matlab Functions. Technical Report 2011-01. Graduate School of Oceanography, University of Rhode Island, Narragansett, RI. 59pp.

Coles, S. An Introduction to Statistical Modelling of Extreme Values Springer Publishers, U.K (2001) Comola, F., Lykke Andersen, T., Martinelli, L., Burcharth, H.F., Ruol, P., 2014. Damage pattern and damage progression on breakwater roundheads under multidirectional waves. Coast. Eng. 83, 24–35.

Dawson, D., Shaw, J., Gehrels, W.R., 2016. Sea-level rise impacts on transport infrastructure: The notorious case of the coastal railway line at Dawlish, England. J.Transp. Geogr. 51, 97–109.

Doney, S.C., Ruckelshaus, M., Duffy, J.E., Barry, J.P., Chan, F., English, C.A., Galindo, H.M., Grebmeier, J.M., Hollowed, A.B., Knowlton, N., Polovina, J., Rabalais, N.N., Donlon, C.; Berruti, B.; Buongiorno, A.; Ferreira, M.-H.; Féménias, P.; Frerick, J.; Goryl, P.; Klein, U.; Laur, H.; Mavrocordatos, C.; et al. The Global Monitoring for Environment and Security (GMES) Sentinel-3 mission. Remote Sens. Environ. 2012, 120, 37–57, ISSN 0034-4257 https://doi.org/10.1016/j.rse.2011.07.024.

Donlon, C.J., Martin, M., Stark, J.D., Roberts-Jones, J., Fiedler, E., Wimmer, W., 2011. The Operational Sea Surface Temperature and Sea Ice Analysis (OSTIA). Remote Sensing of the Environment.

Durrant, T.H., Greenslade, D.J.M., Simmonds, I., 2013. The effect of statistical wind corrections on global wave forecasts. Ocean Model. 70, 116–131.

Egbert, Gary D., and Svetlana Y. Erofeeva. "Efficient inverse modeling of barotropic ocean tides." Journal of Atmospheric and Oceanic Technology 19.2 (2002): 183-204.

Embling, C.B., Sharples, J., Armstrong, E., Palmer, M. R., Scott B. E., Fish behaviour in response to tidal variability and internal waves over a shelf sea bank Prog. Oceanogr., 117 (2013), pp. 106-117

Gerard C. Bond, Evidence for some uplifts of large magnitude in continental platforms, Tectonophysics, Volume 61, Issues 1–3, 1979, Pages 285-305, ISSN 0040-1951, https://doi.org/10.1016/0040-1951(79)90302-0.

Gerkema, T. (2019), An introduction to tides. Cambridge Univ. Press.

Gerritsen, R.A. 2005. What happened in 1953? The Big Flood in the Netherlands in retrospect. Philosophical Transactions of the Royal Society of London, A 363,12711291

Gholami, D. M., and Baharlouii M., Monitoring long-term mangrove shoreline changes along the northern coasts of the Persian Gulf and the Oman sea Emerging Science Journal, 3 (2) (2019), p. 88.

Gomes, Nilton & Neves, Ramiro & Kenov, Isabella & Campuzano, Francisco & Pinto, Lígia.

(2014). Tide and Tidal Currents in the Cape Verde Archipelago. Journal of Integrated Coastal Zone Management. 10.5894/rgci483.

Grédiac, F. S., Effect of sensor noise on the resolution and spatial resolution of displacement and strain maps estimated with the grid method Strain, 50 (1) (2014), pp. 1-27

Gulev, S.K., Grigorieva, V., 2004. Last century changes in ocean wind wave height from Global visual wave data. Geophys. Res. Lett. 31, L24302. https://doi.org/10.1029/2004GL021040.

Habib B. Dieng, Isabelle Dadou, Fabien Léger, Yves Morel, Julien Jouanno, Florent Lyard, Damien Allain, Sea level anomalies using altimetry, model and tide gauges along the African coasts in the Eastern Tropical Atlantic Ocean: Inter-comparison and temporal variability, Advances in Space Research, Volume 68, Issue 2, 2021, Pages 534-552, ISSN 0273-1177, https://doi.org/10.1016/j.asr.2019.10.019.

Hall, J.W., Sayers, P.B., Panzeri, M. and Deakin, R. 2007 Quantitative assessment of driver impacts on future flood risk in England and Wales. Chap. 13 in 'Future flooding and coastal erosion risks' ed. Thorne, C.R., Evans, E.P. and PenningRowsell, E.C. Thomas Telford. 514pp.

Hersbach, H., Bell, B., Berrisford, P., Biavati, G., Horányi, A., Muñoz Sabater, J., Nicolas, J., Peubey, C., Radu, R., Rozum, I., Schepers, D., Simmons, A., Soci, C., Dee, D., Thépaut, J-N. (2018): ERA5 hourly data on single levels from 1979 to present. Copernicus Climate Change Service (C3S) Climate Data Store (CDS). (Accessed on 31-May-2021), 10.24381/cds.adbb2d47.

Hinton, C., Townend, I.H. and Nicholls, R.J. 2007 Coastal Processes. Chap. 9 in ''Future flooding and coastal erosion risks' ed. Thorne, C.R., Evans, E.P. and PenningRowsell, E.C. Thomas Telford. 514pp.

Hoegh-Guldberg, O., Bruno, J.F., 2010. The impact of climate change on the world's marine ecosystems. Science 328, 1523–1528. International Committee on Surveying & Mapping, 2009. Australian Map and Spatial Data Horizontal Accuracy Standard.

Hoitink, A.J.F., Peters, H.C., Schroevers, M. Field verification of ADCP surface gravity wave elevation spectra J. Atmos. Ocean. Technol., 24 (5) (2007), pp. 912-922

Huthnance, J. M. (1973) - Tidal current asymmetries over the Norfolk sand-banks. Estuarine and Coastal Marine Science, 1(1):89–99. DOI: 10.1016/0302-3524(73)90061-3

IPCC, 2013. Climate Change 2013: the Physical Science Basis. Contribution of Working

Group I to the Fifth Assessment Report of the Intergovernmental Panel on Climate Change. Cambridge University Press, Cambridge, United Kingdom and New York, NY, USA.

IPCC, 2014. IPCC. Climate Change 2014: Synthesis Report. Contribution of Working Groups I; II and III to the Fight Assessment Report of the Intergovernmental Panel on Climate Change [core Writing Team; RK Pachauri and LA Meyer] Tech. Rep. IPCC, Geneva; Switzerland (2014).

Janssen, Hanneke (2008). Reconstructing Reality: Environment-Induced Decoherence, the Measurement Problem, and the Emergence of Definiteness in Quantum Mechanics. [Preprint] URL: http://philsci-archive.pitt.edu/id/eprint/4224 (accessed 2020-12-07).

Jenkins, G., Ester Brito, Emanuel Soares, Sen Chiao, Jose Lima, Benvendo Tavares, Angelo Cardoso, Francisco Evora, and Maria Monteiro. "Hurricane Fred (2015): Cape Verde's First Hurricane in modern times: Observations, impacts, and lessons learned" Bulletin of the American Meteorological Society (2018): 2603-2618. doi:https://doi.org/10.1175/BAMS-D-16-0222.1

Kim, S.W., Suh, K.D., 2014. Determining the stability of vertical breakwaters against sliding based on individual sliding distances during a storm. Coast. Eng. 94, 90–101.

Kirshen, P., Watson, C., Douglas, E. et al. Coastal flooding in the Northeastern United States due to climate change. Mitig Adapt Strateg Glob Change 13, 437–451 (2008). https://doi.org/10.1007/s11027-007-9130-5

Knott, J.F., Elshaer, M., Daniel, J.S., Jacobs, J.M., Kirshen, P., 2017. Assessing the effects of rising groundwater from sea level rise on the service life of pavements in coastal road infrastructure. Transp. Res. Rec. 2639 (1), 1–10.

Komen, G.J., Cavaleri, L., Donelan, M., Hasselmann, K., Hasselmann, S. & Janssen, P.A.E.M.1994 Dynamics and modelling of ocean waves. Cambridge University Press. 532pp.

Le Provost, C., Bennett, A. F., Cartwright, D. E., Ocean tides for and from TOPEX/Poseidon, Science 267: 639-642, 1995.

Lewis, M., Schumann, G., Bates, P., Horsburgh, K., Understanding the variability of an Extreme storm tide along a coastline, Estuarine, Coastal and Shelf Science, Volume 123, 2013, Pages 19-25, ISSN 0272-7714, https://doi.org/10.1016/j.ecss.2013.02.009.

Lopes, António & Tenreiro Machado, José. (2017). Tidal Analysis Using Time–Frequency Signal Processing and Information Clustering. Entropy. 19. 390. 10.3390/e19080390.

Mariana Bernardino, Liliana Rusu, C. Guedes Soares, Evaluation of the wave energy

resources in the Cape Verde Islands, Renewable Energy, Volume 101, 2017, Pages 316-326, ISSN 0960-1481, https://doi.org/10.1016/j.renene.2016.08.040.

Mendes, V. B., Barbosa, S. M., Romero, I., Madeira, J., Brum da Silveira A., Vertical land motion and sea level change in Macaronesia, Geophysical Journal International, Volume 210, Issue 2, August 2017, Pages 1264–1280, https://doi.org/10.1093/gji/ggx229.

Mertsz, Françoise (2012). GLOBAL OCEAN GRIDDED L4 SEA SURFACE HEIGHTS AND DERIVED VARIABLES REPROCESSED (1993-ONGOING). https://sextant.ifremer.fr/record/bd5a176b-350e-4d5f-8683-da457637bdcb/. Accessed on 31-May-2021.

Mittelstaedt, E. (1991). The ocean boundary along the northwest African coast: Circulation and oceanographic properties at the sea surface. Progress in Oceanography, 26, 307 – 355.

Mørk, Gunnar & Barstow, Steve & Kabuth, Alina & Pontes, M.. (2010). Assessing the Global Wave Energy Potential. ASME 2010 29th International Conference on ocean, offshore and Arctic Engineering. 3. 10.1115/OMAE2010-20473.

National Research Council, 2009. Mapping the Zone: Improving Flood Map Accuracy. The National Academies Press, Washington, DC.

Neumann, B., Vafeidis, A.T., Zimmermann, J., Nicholls, R.J., 2015. Future coastal population growth and exposure to sea-level rise and coastal flooding-a global assessment. PLoS-ONE 10 (3), e0118571.

Nicholls, R.J., 2002. Analysis of global impacts of sea-level rise: a case study of flooding. Phys. Chem. Earth 27 (32), 1455–1466.

Nicholls, R.J., Cazenave, A., 2010. Sea-level rise and its impact on coastal zones. Science 328, 1517–1520.

Nieto-Borge, J.C., Guedes-Soares, C., 2000. Analysis of directional wave fields using X-band navigation radar. Coast. Eng. 40, 375–391.

NOAA National Centers for Environmental Information (NCEI), 2018. U.S. Billion-dollar weather and climate disasters (2018). Retrieved from NOAAwebsite: https://www.ncdc.noaa.gov/billions/.

Nodoushan E. J., Monthly forecasting of water quality parameters within bayesian networks: a case study of honolulu, pacific ocean Civil Engineering Journal, 4 (1) (2018), p. 188.

Onorato, V. Polnikov, D. Resio, W.E. Rogers, A. Sheremet, J. McKee Smith, H.L. Tolman,

G.van Vledder, J. Wolf, I. Young 2007 Wave modelling – the state of the art. Progress in Oceanography, 75, 603–674.

Oppenheimer, M. et al., 2019: Sea Level Rise and Implications for Low Lying Islands, Coasts and Communities. In: IPCC Special Report on the Ocean and Cryosphere in a Changing Climate [Pörtner, H.-O., D.C. Roberts, V. Masson-Delmotte, P. Zhai, M. Tignor, E. Poloczanska, K. Mintenbeck, M. Nicolai, A. Okem, J. Petzold, B. Rama, and N. Weyer (eds.)]. In Press, pp. 321–445

PANA, 2004. Segundo Plano de Acção Nacional para o Ambiente 2004-2014, Ministry of Agriculture, Food and the Environment, Praia (Republic of Cape Verde) 218 p.

Park, Joseph & Heitsenrether, Robert & Sweet, William. (2014). Water Level and Wave Height Estimates at NOAA Tide Stations from Acoustic and Microwave Sensors. Journal of Atmospheric and Oceanic Technology. 31. 2294-2308. 10.1175/JTECH-D 14-00021.1.

Passaro, M., Cipollini, P., Vignudelli, S., Quartly, G.D., Snaith, H.M., 2014. ALES: a multi mission adaptive subwaveform retracker for coastal and open ocean altimetry. Remote Sens. Environ. 145 (1), 173–189. https://doi.org/10.1016/j.rse.2014.02.008.

Pattrick, P., and Strydom N., Recruitment of fish larvae and juveniles into two estuarine nursery areas with evidence of ebb tide use. Estuarine Coastal and Shelf Science, 149 (2014), pp.120-132

Pawlowicz, R.; Beardsley, B.; Lentz, S. (2002) - Classical tidal harmonic analysis including error estimates in MATLAB using T_TIDE. Computers & Geosciences, 28(8):929-937. DOI: 10.1016/S0098-3004(02)00013-4

Permanent Service for Mean Sea Level (PSMSL), 2021, "Revised Local Reference for Palmeira", Retrieved 20 Oct 2021 from http://www.psmsl.org/data/obtaining/rlr.diagrams/1914.php.

Pingree, R. D.; Maddock, L. (1980) - Tidally induced residual flows around an island due to both frictional and rotational effects. Geophysical Journal of the Royal Astronomical Society, 63(2):533–546. DOI: 10.1111/j.1365-246X.1980.tb02636.x

Plant, W., Keller, W., Hayes, K., Chatham, C., 2008. Measuring and modeling the NRCS of the sea for backscatter. IEEE Int. Geosci. Remote Sens. Symp. 4, 65–68.

Prandi, P., Cazenave, A., and Becker, M. (2009), Is coastal mean sea level rising faster than the global mean? A comparison between tide gauges and satellite altimetry over 1993–2007, *Geophys. Res. Lett.*, 36, L05602, doi:10.1029/2008GL036564.

Ramalho R, Helffrich G, Schmidt DN, Vance D. 2010. Tracers of uplift and subsidence in the

Cape Verde archipelago. Journal of the Geological Society 167(3): 519–538. https://doi.org/10.1144/0016-76492009-056.

Ramalho, Ricardo. (2011). Building the Cape Verde Islands. 10.1007/978-3-642-19103-9.

Ray, R. D.: 1999, A global ocean tide model from Topex/Poseidon altimetry, NASA Tech. Memo. 209478, Goddard Space Flight Center, Greenbelt, 58 pp.

R.F. McLean, A. Tsyban, V. Burkett, J.O. Codignott, D.L. Forbes, N. Mimura, V. Ittekkot, Coastal zones and Marine ecosystems. Climate change 2001: impacts, in: Adaptation and Vulnerability, pp. 343–379, Cambridge, UK, 2001.

R.J. Nicholls, N. Marinova, J.A. Lowe, S. Brown, P. Vellinga, D. De Gusmão, R.S.J. Richardson, A., Poloczanska, E., 2008. OCEAN SCIENCE: under-resourced, under threat. Science 320 (5881), 1294–1295.

Rosenzweig, C., Karoly, D.J., Vicarelli, M., Neofotis, P., Wu, Q., Casassa, G., Menzel, A., Root, T.L., Estrella, N., Seguin, B., Tryjanowski, P., Liu, C., Rawlins, S., Imeson, A., 2008. Attributing physical and biological impacts to anthropogenic climate change. Nature 453, 353–357.

Sallenger Jr., A.H., 2000. Storm impact scale for barrier islands. J. Coast Res. 890–895.

Sangdon So, Braulio Juarez, Arnoldo Valle-Levinson, Matlack E. Gillin, Storm surge from Hurricane Irma along the Florida Peninsula, Estuarine, Coastal and Shelf Science, Volume 229, 2019, 106402, ISSN 0272-7714, https://doi.org/10.1016/j.ecss.2019.106402.

Shepard, C.C., Crain, C.M., Beck, M.W., 2011. The protective role of coastal marshes: a Systematic review and meta-analysis. PloS One 6, e27374.

Spalding, M.D., Ruffo, S., Lacambra, C., Meliane, I., Hale, L.Z., Shepard, C.C., Beck, M. W., 2014. The role of ecosystems in coastal protection: adapting to climate change and coastal hazards. Ocean Coast Manag. 90, 50–57.

Sydeman, W.J., Talley, L.D., 2012. Climate change impacts on marine ecosystems. Ann. Rev. Marine Sci. 4, 11–37.

Taburet, G., Sanchez-Roman, A., Ballarotta, M., Pujol, M.-I., Legeais, J.-F., Fournier, F., et al. (2019). DUACS DT2018: 25 years of reprocessed sea level altimetry products. Ocean Sci 15, 1207–1224. doi: 10.5194/os-15-1207-2019

Thompson, P. R., Hamlington, B. D., Landerer, F. W., and Adhikari, S. (2016), Are long tide gauge records in the wrong place to measure global mean sea level rise?, *Geophys. Res. Lett.*, 43, 10,403– 10,411, doi:10.1002/2016GL070552.

Tolman, H.L., 2009. User manual and system documentation of WAVEWATCH III TM version 3.14, Tech. Note 276, NOAA/NWS/NCEP/MMAB.

The WISE Group, Cavaleri, L., Alves, J.-H.G.M., Ardhuin, F., Babanin, A., Banner, M., Belibassakis, K., Benoît, M., Donelan, M., Groeneweg, J., Herbers, T.H.C., Hwang, P., Janssen, P.A.E.M., Janssen, T., Lavrenov, I.V., Magne, R., Monbaliu, J., Onorato, M., Polnikov, V., Resio, D., et al., 2007, "Wave modelling - The state of the art", Progress in Oceanography, vol. 75, no. 4, pp. 603-674.

Tucker, M., and E. Pitt Waves in Ocean Engineering, Voume 5 (Elsevier Ocean Engineering Series) Elsevier Science (2001).

Villarini, G., and G. A. Vecchi, 2013: Projected increases in North Atlantic tropical cyclone intensity from CMIP5 models. J. Climate, 26, 3231–3240, https://doi.org/10.1175/JCLI-D-12-00441.1

Winter, A.O., Motley M. R., and M.O. Eberhard Tsunami-like wave loading of individual BridgeComponentsJ.BridgeEng., 23 (2) (2017), Article 04017137, 10.1061/(ASCE) BE.1943-5592.0001177 https://ascelibrary.org/doi/abs/10.1061/%28ASCE%29BE.1943-5592.0001177

Wolf, J. 2008 Coupled wave and surge modeling and implications for coastal flooding Advances in Geosciences. 17, 1-4.

Woodworth, P.L., Melet, A., Marcos, M. et al. Forcing Factors Affecting Sea Level Changes at the Coast. Surv Geophys 40, 1351–1397 (2019). https://doi.org/10.1007/s10712019-09531-1.

World Bank Group. 2015. Managing Coastal Risks in West Africa. West Africa Coastal Areas Management Program Knowledge Sheet;3. World Bank, Washington, DC. © World Bank. https://openknowledge.worldbank.org/handle/10986/24281 License: CC BY 3.0 IGO.

WTTC (World Travel and Tourism Council). 2018. Travel and Tourism Economic Impact 2018: Cape Verde. WTTC: London.

Xiao, H W. Huang, Q. Chen Effects of submersion depth on wave uplift force acting on Biloxi Bay Bridge decks during Hurricane Katrina Comput. Fluid, 39 (8) (2010), pp. 1390-1400,10.1016/j.compfluid.2010.04.009 https://www.sciencedirect.com/science/article/abs/pii/S004579301000085X

Young, I.R., Zieger, S., Babanin, A., 2011. Global trends in wind speed and wave height. Science 332(6028)., 451–455.

Zou, Q.P., Chen, Y., Cluckie, I., Hewston, R., Pan, S., Peng, Z., Reeve, D., 2013. Ensemble prediction of coastal flood risk arising from overtopping by linking meteorological, ocean, coastal and surf zone models. Q. J. Roy. Meteorol. Soc. 139 (671), 298–313.